

TOP FILE COPY

2

MISCELLANEOUS PAPER HL-89-7



US Army Corps of Engineers

AD-A216 316



SCHEMATIC NUMERICAL MODELING OF HARBOR DEEPENING EFFECTS ON SEDIMENTATION CHARLESTON, SOUTH CAROLINA

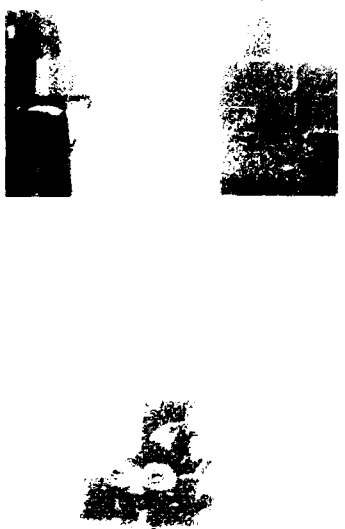
by

Allen M. Teeter, Walter Pankow

Hydraulics Laboratory

DEPARTMENT OF THE ARMY

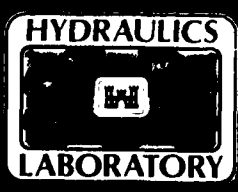
Waterways Experiment Station, Corps of Engineers
3909 Halls Ferry Road, Vicksburg, Mississippi 39180-6199



September 1989
Final Report

Approved For Public Release. Distribution Unlimited

SDTIC
ELECTE
DEC 29 1989
S E D



Prepared for US Army Engineer District, Charleston
Charleston, South Carolina 29402-0919

89 12 28 095

• •

Destroy this report when no longer needed. Do not return
it to the originator.

The findings in this report are not to be construed as an official
Department of the Army position unless so designated
by other *authorized documents*.

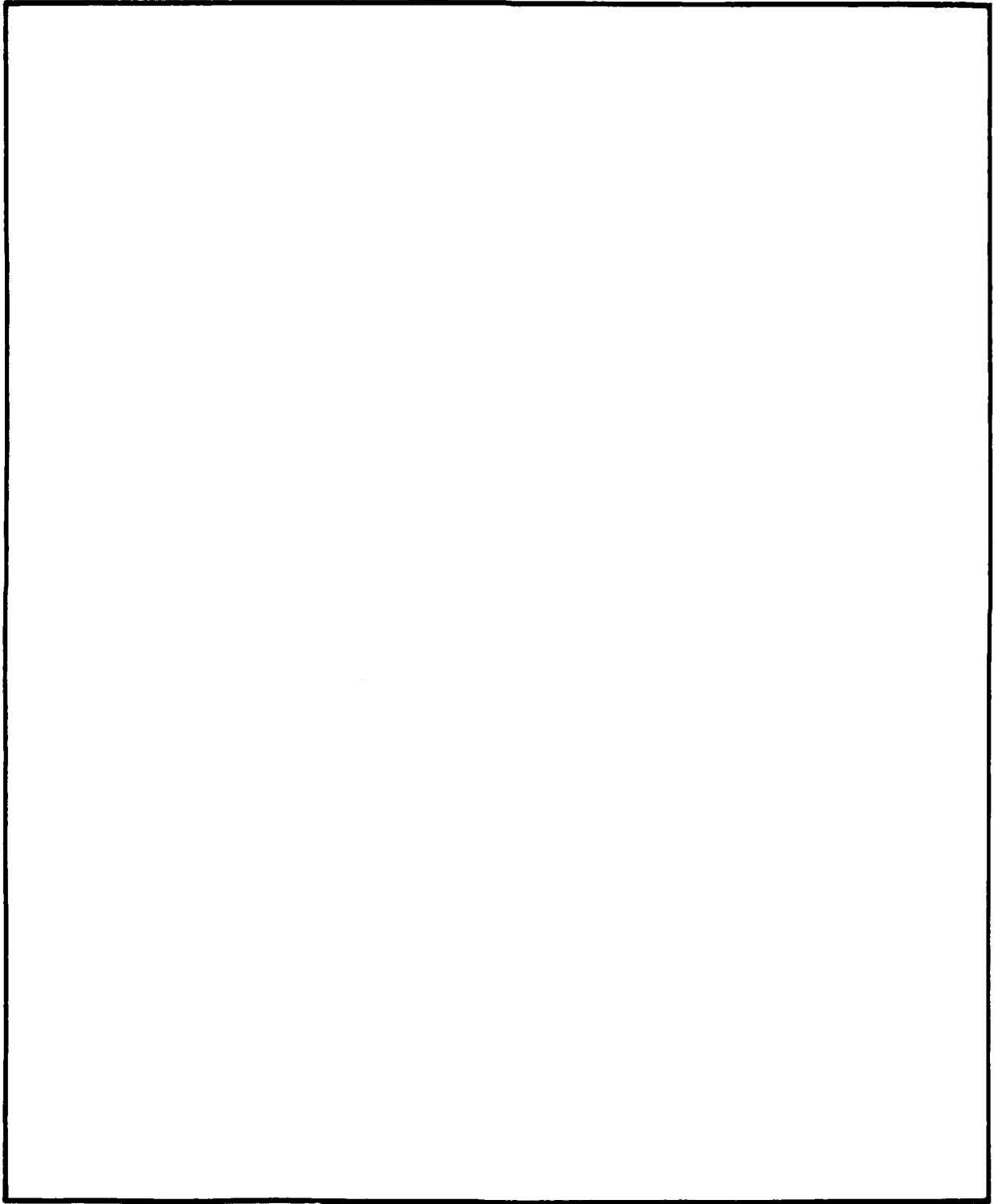
The contents of this report are not to be used for
advertising, publication, or promotional purposes.
Citation of trade names does not constitute an
official endorsement or approval of the use of
such commercial products.

Unclassified

SECURITY CLASSIFICATION OF THIS PAGE

REPORT DOCUMENTATION PAGE				Form Approved OMB No. 0704-0188	
1a. REPORT SECURITY CLASSIFICATION Unclassified		1b. RESTRICTIVE MARKINGS			
2a. SECURITY CLASSIFICATION AUTHORITY		3. DISTRIBUTION / AVAILABILITY OF REPORT Approved for public release; distribution unlimited.			
2b. DECLASSIFICATION / DOWNGRADING SCHEDULE					
4. PERFORMING ORGANIZATION REPORT NUMBER(S) Miscellaneous Paper HL-89-7		5. MONITORING ORGANIZATION REPORT NUMBER(S)			
6a. NAME OF PERFORMING ORGANIZATION USAEWES Hydraulics Laboratory		6b. OFFICE SYMBOL (if applicable) CEWES-HE-P	7a. NAME OF MONITORING ORGANIZATION		
6c. ADDRESS (City, State, and ZIP Code) 3909 Halls Ferry Road Vicksburg, MS 39180-6199		7b. ADDRESS (City, State, and ZIP Code)			
8a. NAME OF FUNDING / SPONSORING ORGANIZATION USAED, Charleston		8b. OFFICE SYMBOL (if applicable)	9. PROCUREMENT INSTRUMENT IDENTIFICATION NUMBER		
8c. ADDRESS (City, State, and ZIP Code) PO Box 919 Charleston, SC 29402-0919		10. SOURCE OF FUNDING NUMBERS			
		PROGRAM ELEMENT NO.	PROJECT NO.	TASK NO.	WORK UNIT ACCESSION NO.
11. TITLE (Include Security Classification) Schematic Numerical Modeling of Harbor Deepening Effects on Sedimentation, Charleston, South Carolina					
12. PERSONAL AUTHOR(S) Teeter, Allen M., and Pankow, Walter					
13a. TYPE OF REPORT Final report		13b. TIME COVERED FROM _____ TO _____	14. DATE OF REPORT (Year, Month, Day) September 1989		15. PAGE COUNT 90
16. SUPPLEMENTARY NOTATION Available from National Technical Information Service, 5285 Port Royal Road, Springfield, VA 22161.					
17. COSATI CODES			18. SUBJECT TERMS (Continue on reverse if necessary and identify by block number) Channel deepening Estuarine shoaling Charleston Harbor Sedimentation modeling Cooper River		
FIELD	GROUP	SUB-GROUP			
19. ABSTRACT (Continue on reverse if necessary and identify by block number) This report describes schematic numerical model analysis of harbor channel deepening effects on sedimentation for Charleston Harbor, Charleston, SC. The harbor channel is being deepened from -35 to -40 ft mean low water, and the harbor freshwater inflow has been recently decreased from about 15,600 to 4,500 cfs average. Existing hydraulic and sediment information was used. The schematic numerical modeling approach was selected because no simpler (analytical or steady state) shoaling prediction was known which could account for both channel deepening and altered inflow conditions. A two-dimensional laterally averaged numerical model Fine-Grained Bed Sediment (FIBS) with 1- and 2-mile node spacing was used. Harbor deepening was predicted to increase dredging requirements by about 15 percent for 4,500-cfs inflow. The centroid of the shoaling distribution was predicted to move upstream about 7 miles for this flow. (K.F.)					
20. DISTRIBUTION / AVAILABILITY OF ABSTRACT <input checked="" type="checkbox"/> UNCLASSIFIED/UNLIMITED <input type="checkbox"/> SAME AS RPT. <input type="checkbox"/> DTIC USERS			21. ABSTRACT SECURITY CLASSIFICATION Unclassified		
22a. NAME OF RESPONSIBLE INDIVIDUAL			22b. TELEPHONE (Include Area Code)		22c. OFFICE SYMBOL

SECURITY CLASSIFICATION OF THIS PAGE



SECURITY CLASSIFICATION OF THIS PAGE

PREFACE

The prediction of deepening effects on sedimentation, documented in this report, was performed for the US Army Engineer District, Charleston, and included use of techniques recently developed under the Improvement of Operations and Maintenance Techniques (IOMT) research program sponsored by the Headquarters, US Army Corps of Engineers, under IOMT Work Unit No. 31765, "Fine-Grained Shoaling in Navigation Channels." This study was conducted in the Hydraulics Laboratory (HL) of the US Army Engineer Waterways Experiment Station (WES) during the period January 1986 to September 1988 under the general supervision of Messrs. Frank A. Herrmann, Jr., Chief, HL; Richard A. Sager, Assistant Chief, HL; William H. McAnally, Jr., Chief, Estuaries Division; and George M. Fisackerly, Chief, Estuarine Processes Branch.

The study was conducted and this report prepared by Mr. Allen M. Teeter, Estuarine Processes Branch. Mr. Walter Pankow, Estuarine Processes Branch, assisted in the preparation of this report. Mr. Howard A. Benson, Estuarine Processes Branch, was the field engineer for the field data collection which preceded this study. Field technicians who collected data included Messrs. David Crouse (retired), Joseph W. Parman, James T. Hilbun, Samuel E. Varnell, Billy G. Moore, John T. Cartwright, Douglas M. White, and John S. Ashley, all with the Estuaries Division. Mrs. Clara Coleman, Estuarine Processes Branch, reduced the data to computer files. Mrs. Marsha C. Gay, Information Technology Laboratory, WES, edited this report.

The Charleston District contact persons were Messrs. Lincoln Blake, Robert Billue, and James Joslin.

Commander and Director of WES during preparation of this report was COL Larry B. Fulton, EN. Technical Director was Dr. Robert W. Whalin.

Accession For	
NTIS GRA&I	<input checked="" type="checkbox"/>
DTIC TAB	<input type="checkbox"/>
Unannounced	<input type="checkbox"/>
Justification	
By _____	
Distribution/	
Availability Codes	
Dist	Avail and/or Special
A-1	



CONTENTS

	<u>Page</u>
PREFACE.....	1
CONVERSION FACTORS, NON-SI TO SI (METRIC) UNITS OF MEASUREMENT.....	4
PART I: INTRODUCTION.....	5
Background.....	5
Purpose.....	5
Scope.....	5
PART II: STUDY DESCRIPTION.....	7
Prototype Conditions.....	7
Background Studies and Information.....	7
Numerical Modeling Methods.....	9
PART III: TEST CONDITIONS.....	12
Channel and Inflow Conditions.....	12
Tide and Sediment Conditions.....	12
General Test Procedures.....	13
PART IV: RESULTS.....	15
Verification Results.....	15
Test Results.....	16
PART V: DISCUSSION.....	18
PART VI: CONCLUSIONS.....	20
REFERENCES.....	22
TABLES 1-8	
FIGURES 1-20	
APPENDIX A: SHOALING RATES AT 3,000- to 4,500-CFS INFLOW.....	A1
Purpose.....	A1
Brief Review of Previous Shoaling Analyses.....	A1
Shoaling Processes in Charleston Harbor.....	A3
Prediction Method.....	A4
Expected Shoaling.....	A5
Entrance Channel Shoaling.....	A6
TABLES A1-A2	
APPENDIX B: FLOW AND SALINITY MODEL.....	B1
Equations.....	B1
Boundary Conditions.....	B5
Vertically Stretching Coordinates.....	B6
Solutions of the Equations.....	B7
Integration in Time.....	B8
APPENDIX C: SEDIMENT TRANSPORT MODEL EQUATIONS.....	C1
Characterization of Suspended Sediment.....	C1
Governing Transport Equation.....	C1

	<u>Page</u>
Settling.....	C2
Deposition.....	C3
Resuspension.....	C4
APPENDIX D: FLUID MUD MODELING.....	D1
Background.....	D1
Model Description.....	D3
FIGURES D1-D4	
APPENDIX E: DEFINITION OF TERMS.....	E1
APPENDIX F: NOTATION.....	F1

CONVERSION FACTORS, NON-SI TO SI (METRIC)
UNITS OF MEASUREMENT

Non-SI units of measurement used in this report can be converted to SI
(metric) units as follows:

<u>Multiply</u>	<u>By</u>	<u>To Obtain</u>
cubic feet	0.02831685	cubic metres
cubic yards	0.7645549	cubic metres
feet	0.3048	metres
pounds	0.000454	metric tons
pounds per cubic foot	16.02	grams per litre
miles (US statute)	1.6093	kilometres
square feet	0.09290341	square metres

SCHEMATIC NUMERICAL MODELING OF HARBOR DEEPENING EFFECTS
ON SEDIMENTATION, CHARLESTON, SOUTH CAROLINA

PART I: INTRODUCTION

Background

1. The US Army Engineer Waterways Experiment Station (USAEWES) Hydraulics Laboratory (HL) has studied the effects of the Cooper River redirection on sediment flushing, mixing, and circulation in Charleston Harbor, Charleston, SC (Teeter 1989). An associated study task was to reexamine the possible effects of ongoing Charleston Harbor navigation channel deepening on dredging requirements for the harbor. Previously, physical model hydrodynamic results were used by WES to qualitatively assess the effect of harbor deepening on shoaling (Benson 1976).

Purpose

2. The purpose of this study was to predict shoaling for the new project channel at -40 ft mean low water (mlw) and a daily average inflow of 4,500 cfs for the purpose of providing information with which the US Army Engineer District (USAED), Charleston, planners can assess disposal site capacity requirements.

Scope

3. The scope of this study included the schematic application of a numerical model using existing hydraulic and sediment information to gage the effects of a 5-ft channel deepening on shoaling rates and distribution in the main portion of the harbor channel. The schematic numerical modeling approach was selected because no simpler (analytical or steady state) shoaling predictor was known which could account for both channel deepening and altered inflow conditions. A two-dimensional laterally averaged model called FIBS (Fine-Gained Bed Sediment) was employed. A limited verification of the schematic model was performed.

4. The effects of redirection on channel shoaling rates were also

tested, incidental to other tests. Salinity* intrusion and stratification were considered by this study, but were based on previous physical model results. Modeling included the effects of circulation, and covered the main harbor channel and upstream river reach to the Pinopolis Dam (Figure 1).

5. This report summarizes the methods and procedures used and the results obtained.

* Unusual terms are listed and defined in Appendix E.

PART II: STUDY DESCRIPTION

Prototype Conditions

6. Charleston Harbor is formed by the junction of the Ashley, Wando, and Cooper Rivers, and is a major South Carolina seaport (Figure 1). Average tide range is 5.3 ft (1.61 m)* at the Customs House at Charleston, located at about river mile 9. Conditions in Charleston Harbor have recently changed as freshwater inflow was reduced by about 71 percent after the 1985 redirection of the Cooper River. The effect of the redirection on shoaling will be a gradual decrease in harbor shoaling over perhaps a decade. Presently, a 5-ft channel deepening is underway in the navigation project, possibly altering shoaling conditions. Therefore, Charleston Harbor is in transition with respect to shoaling, and the only shoaling information available is the dredging records for pre-redirection harbor conditions. Because of the recent changes in harbor conditions caused by the redirection of the Cooper River, this study addressed the effects of both reduced inflow (redirection) and increased channel depths on harbor shoaling.

Background Studies and Information

7. The main sources of information for this study were dredging records (USAED, Charleston, 1966 and I. B. Kyzer**), previous sediment characterization studies (USAED, Charleston, 1954 and Teeter 1989), physical model data (Benson 1976 and USAEWES 1957), and sediment budget studies (Patterson 1983 and Teeter 1989). Two physical models have been used in various harbor studies by USAEWES, including two studies which addressed channel deepening and redirection.

8. In the most recent physical model study, USAEWES tested the effects of a -40 ft mlw channel on tides, currents, and salinities (Benson 1976). Tests were performed with 15,600- and 3,500-cfs inflows, and with -35 and -40 ft mlw channels. The difference between mlw and National Geodetic

* A table of factors for converting non-SI units of measurement to SI (metric) units is found on page 4.

** Meeting with Mr. I. Braxton Kyzer, US Army Engineer District, Charleston, Engineering Division, in April 1986.

Vertical Datum (NGVD) is 1.98 ft. The difference between mlw and the National Geodetic Vertical Datum (NGVD), which is now the standard vertical datum, is 1.98 ft. However, because previous navigation projects used mlw as the vertical datum, this study uses it also. The difference between mlw and mean sea level is 2.5 ft at the Customs House tide gage at Charleston.

9. The physical model study of harbor deepening found a slight increase in tide ranges, very slight increases in currents, and a slight decrease in salinity stratifications near the upper end of the harbor project associated with the channel deepening. The limit of the 100-ppm saltwater intrusion length was predicted to advance about 1 mile after the channel deepening. The study concluded that, based on changes in hydrodynamic conditions, changes in shoaling conditions would be minimal with a tendency for peak shoaling to shift toward the upstream end of the navigation channel.

10. The earliest USAEWES physical model studies examined the effects of the redirection on harbor mixing and shoaling (USAEWES 1957). Tests of flows between 2,500 and 5,000 cfs indicated that the harbor abruptly became well-mixed and sediment flushing improved. Model shoaling tests found that reduction in freshwater inflow from 15,600 to 3,000 cfs (with a corresponding decrease in sediment inflow of 80 percent) reduced shoaling by 92 percent (exclusive of entrance shoaling). The channel deepening from -30 to -35 ft mlw which occurred in the 1940's was found to have had a minimal effect on harbor shoaling.

11. The US Geological Survey (USGS) also studied the effect of redirection on shoaling (Patterson 1983). Dredging records, hydrographic surveys, maps, charts, hydrologic data, unpublished files, and knowledgeable individuals were sources of information for that study. Information on inflow suspended sediment concentrations was compiled. It was predicted that maintenance dredging would be reduced by 40 to 75 percent as a result of the redirection.

12. Some dredged sediment returns to the estuary due to overflows, leaks, or disposal practices. Patterson (1983) estimated this quantity of sediment, termed runback, to be 22 percent of the dredged sediment for the 1965-1984 period. Average annual dredging for this period was 4.81 million cubic yards per year exclusive of the entrance channel.

13. The Cooper River redirection was carried out in late 1985. USAEWES performed field data collection and analysis on current and salinity

conditions before redirection and over a range of inflows from 4,500 cfs to a project base level of 3,000-cfs daily average. A small amount of suspended material data was also collected in the lower harbor: hourly over tidal cycles and composites over lunar days. Suspended sediment concentrations varied between 50 and 350 mg/l at river mile 7 (0.75 depth) over a neap to spring tidal sequence and 4,900-cfs inflow (Figure 2). A storm increased suspended sediment concentrations to about 1,350 mg/l for 2 days at that location. Analysis of suspended sediment data from two surveys at river mile 8 indicated that tidal pumping was the dominant flux component and could operate in either the upstream or seaward directions (Teeter 1989).

14. A study of redirection shoaling reduction between 3,000- and 4,500-cfs daily average inflows predicted a 4 percent difference, from 74 to 70 percent reduction respectively, based on a sediment budget approach (Teeter 1989). That analysis is presented in Appendix A.

Numerical Modeling Methods

15. The numerical sediment model used in this study, FIBS, was an enhancement to the numerical hydrodynamic and salinity intrusion model system (SIMS 1) developed for the Cooper River redirection study (Teeter 1989). The FIBS model has the capability to predict flow and transport in an estuarine setting, and stresses fluid mud bed processes. The model numerically solved laterally averaged dynamic differential equations for flow continuity, conservation of horizontal momentum, and conservation of mass (salt and sediment) over the interval between the water surface and the channel bottom, and along the length of the channel. The horizontal momentum equation included nonlinear advection and quadratic bottom friction terms. Appendix B describes details of the flow and salt transport modeling.

16. The basic laterally averaged two-dimensional flow and salt transport equations have been presented previously by various authors. Such systems of equations have been shown to reproduce estuarine circulation driven by density currents and tidal propagation. In FIBS, additional terms were included in the conservation of sediment equation to account for sediment dynamics. Sediment dynamic processes for settling, deposition, and erosion were described by a set of algebraic equations which depended on bed shear stress, suspended sediment concentration, bed sediment concentration (or density) and

sediment-dependent coefficients and will be discussed later.

17. Density terms were included in the momentum equation, coupling the salt transport and momentum equations. The standard assumptions of incompressibility, hydrostatic pressure, and negligible vertical momentum were adapted, allowing vertical current velocities to be computed using a form of the continuity equation.

18. Transport equations for turbulent kinetic energy with production and dissipation terms were also solved in the model. The vertical distribution of eddy coefficients varied according to an analytic expression. For simplicity, turbulence closure to momentum and transport equations was not implemented for this study. Vertical distributions of eddy diffusion were used in the calculations of effective eddy diffusivity coefficients.

19. Vertical eddy diffusivities for mass and momentum were functions of input coefficients, depth, and Richardson number. Vertical density and velocity gradients were used to dynamically calculate Richardson numbers, and adjust vertical eddy diffusivities for mass and momentum according to an analytical expression.

20. An ocean boundary condition was formulated for FIBS to minimize reflection of long waves (surges) originating within the flow domain. The nonreflecting model ocean boundary permitted the dynamic equilibrium or repeating tide condition to be attained much more quickly than with an ocean water-level boundary specification fixed at each time level. Dynamic equilibrium was reached in about two tidal cycles.

21. FIBS solves equations over finite elements using a method of weighted residuals (orthogonal collocation). The flow domain was discretized as a series of elements consisting of 15 computational points, configured as five horizontal rows of three points (or nodes). Each node consisted of a vertical column of five computational points. Breadth at each node varied vertically as a quadratic function of depth. Model equations were solved implicitly over elements. Time integration was performed using an explicit method described in Appendix B.

22. The sediment algorithm for FIBS was recently developed at USAEWES as part of a research work unit on fine-grained sediment. A number of associated algebraic equations were solved at each time-step for

- a. Settling velocity W_s^* of sediments as a function of suspension concentration C .
- b. Depositional probability P as a function of bed shear stress τ_b and critical shear stress for deposition τ_{cd} .
- c. Critical shear stresses for particle τ_c and significant erosion τ_{ch} as functions of the bed density C_s .
- d. Particle and significant erosion as functions of critical and bed shear stresses.

Definitions for many of these terms and details on sediment transport modeling are presented in Appendix C.

23. The FIBS model accounts for changes in bed concentration or density and thickness of a fluid mud layer at the surface of the bed. The bed was defined as the elevation where horizontal motion was zero, and where sediment concentration was greater than a specified value (70 g/l). The fluid mud layer was defined as that top part of the bed where sediment concentrations were less than the fully settled condition (300 g/l). Two additional bed-sediment layers were included in the model below the fluid mud layer.

24. Formation and densification of the fluid mud layer were computed using differential equations for continuity and conservation of mass, and solved over the variable fluid mud vertical domain below the elevation of the bed. A numerical scheme similar to that used for the flow domain was used to solve over the vertical, five-computational-point fluid mud layers at each node. An algebraic expression was used to calculate settling rates W_h as a function of bed concentration in the hindered-settling range of concentrations C_s . Details on the fluid mud model are given in Appendix D.

* For convenience, symbols and unusual abbreviations are listed and defined in the Notation (Appendix F).

PART III: TEST CONDITIONS

25. Test conditions consisted of two groups: (a) channel and inflow conditions and (b) tide and sediment conditions.

Channel and Inflow Conditions

26. Schematic numerical modeling was employed, using limited spatial resolution appropriate for system definition in which the sediment information was limited. The numerical mesh covered the harbor from river mile 1 to river mile 25 at 1-mile cross-section intervals, and from river mile 25 to Pinopolis (river mile 57) in 2-mile cross-section intervals (Figure 1). Figure 3 shows the cross-sectional areas at locations along the estuary and river. The numerical mesh describing estuarine geometry was not extensive and did not include branches to represent the East Branch Cooper River or the Back River Reservoir.

27. During the period 1965-1984, the project channel was -35 ft mlw, plus -4 ft of advanced maintenance and -2 ft of allowable overdepth dredging for a maximum channel depth of -41 ft mlw. The Navy channel above the ordinance reach (river miles 20-24) had a maximum depth of -37 ft mlw (-35 ft project depth plus -2 ft advanced maintenance). Since 1985, overdepth dredging was reduced, and the maximum channel depth was -39 ft mlw. All model channel depths were specified as 2 ft less than the maximum depths to represent average channel depths during a dredging cycle. The following tabulation shows channel depths for the three harbor conditions modeled:

Condition	Inflow cfs	Depths, ft mlw			
		Prototype		Model Channel	
		Project	Maximum	Harbor	Navy
Base	15,600	-35	-41	-39	-37
Base	4,500	-35	-39	-37	-35
Plan	4,500	-40	-44	-42	-40

Tide and Sediment Conditions

28. Table 1 describes seven tidal and sediment conditions varied for

test prediction and sensitivity analysis. Table 1 also defines the five combinations of tidal and sediment conditions used for test predictions. These are discussed in Part V.

29. Other sediment parameters were constant for all tests. For the 15,600-cfs base model test, initial suspended sediment concentration was 250 ppm. Suspended sediment concentrations at the ocean and upstream boundaries were set at 165 ppm and 14 ppm, respectively. The latter is the average suspended sediment concentration at the Pinopolis inflow to the Cooper River, according to USGS data.

30. For 4,500-cfs base and plan model tests, initial suspended sediment concentrations were 75 ppm. Suspended sediment concentrations at the ocean and upstream boundaries were set at 50 ppm and 14 ppm, respectively.

31. For lack of site-specific information, known sediment characteristics of similar estuarine sediments were used as guidance in selecting the necessary sediment parameters for this study. Preliminary sensitivity tests on sediment parameters were also used to guide sediment parameter selection.

General Test Procedures

32. Model test sequences were used to represent the prototype situation where greater than average concentrations of sediment materials are in suspension and generally erode during spring tidal conditions, while less than average concentrations of sediment materials are in suspension and generally deposit during neap tidal conditions. Net sedimentary conditions are erosional between neap and spring tide ranges, and depositional between spring and neap tide ranges. During these sequences, suspended sediments are added upstream and exchanged with the ocean, depending on sediment flushing conditions in the harbor. Prototype suspended sediment loads thus constantly change over tides and over lunar months, and the balance between erosion and deposition leads to net shoaling or erosion over time.

33. The FIBS numerical model was applied in test sequences of three steps to represent prototype suspended sediment variability.

- a. The first computational step was used to start model hydrodynamics and gain repeating tidal conditions in the model. An M2 lunar tide was applied at the ocean boundary, the appropriate freshwater inflow was introduced upstream at Pinopolis, and model computations were carried out for two tidal cycles.

- b. The second model computational step was an erosional phase of one tidal cycle produced by decreasing fluid mud density to allow erosion.
- c. The third and final computational step was a two-to-four tidal cycle equilibrium phase. Shoaling rates were determined at the end of the test sequences.

PART IV: RESULTS

Verification Results

34. Model tidal propagation was verified for the 15,600- and 4,500-cfs base conditions using physical model results. The sediment transport model was verified to observed field shoaling rates under the conditions of 15,600-cfs inflow and -35 ft mlw project channel. The average annual maintenance dredging records from 1965-1984 were used for the shoaling verification. Dredging at Shipyard Creek and the entrance channel was not included in the verification.

Tidal hydraulics

35. Tables 2-4 show physical and numerical model tide results along the main channel for the 15,600-cfs base, 4,500-cfs base, and 4,500-cfs plan conditions, respectively. Figure 4 shows the tidal envelope swept out by instantaneous water-surface profiles for physical model tests. Figures 5-7 show the numerical and physical model tidal envelopes for the 15,600-cfs base, 4,500-cfs base, and 4,500-cfs plan conditions, respectively. Tidal reproduction in the schematic numerical model was acceptable.

Salinity

36. Physical model data were used to drive salinity conditions in the numerical model. Previous Cooper River studies adopted chlorinity to represent salinity because the concern at the limit of intrusion focused on chlorides. Figures 8-10 show salinity distributions along the harbor channel in the numerical model for the 15,600-cfs base, 4,500-cfs base, and 4,500-cfs plan conditions, respectively. Physical model salinity results were used to initialize and update salinity distributions, forcing numerical model and physical model results to be very similar. It was not within the scope of this study to predict the effects of deepening on salinity distributions. The physical model has been the best tool applied to predict salinity effects of channel deepening and was relied upon for this study.

Shoaling

37. Shoaling verification results are shown in Table 5 and Figure 11. They show the average prototype dredging rates along the harbor channel for the 1965-1984 period, and the values predicted by the model for 15,600-cfs inflow and -35 ft mlw channel condition. The agreement between the overall

model and prototype shoaling magnitudes was excellent. Upstream of river mile 11, the general shape of the verification shoaling distribution was similar to, but smoother than, the prototype distribution. Between river miles 6 and 10, the model shoaling distribution was spatially out of phase with the prototype distribution probably due to the lack of branching in the model. Although the comparison of shoaling distributions was rather poor, it was considered sufficient for this study. Heavy shoaling areas in the model occurred where maximum near-bed velocities were upstream, and near the point of zero tidal-averaged flow (the null point). Maximum near-bed velocities and tidal-averaged flows are discussed in the next section.

Test Results

38. Vertical circulation and tidal pumping greatly affect harbor shoaling. Circulation reflects density and geometry effects, and often acts to trap sediments in estuaries. Figures 12-14 show tidal-averaged circulation in the harbor area for the 15,600-cfs base, 4,500-cfs base, and 4,500-cfs plan conditions, respectively. Near-bed tidal-averaged velocities were very low at river miles 9-23 for 15,600-cfs base, and at river miles 7-12 for 4,500-cfs base and plan conditions.

39. Maximum near-bed velocities reflect density and tidal effects, and indicate the probable direction of tidal pumping of suspended material. Figures 15-17 show tidal maximum near-bed velocities squared (proportional to maximum shear stress) and the direction of maximum velocities for the 15,600-cfs base, 4,500-cfs base, and 4,500-cfs plan conditions, respectively. Note that reversals in the maximum velocity squared values reflect relatively small differences in longitudinal values and in ebb/flood values. Tidal-average suspended sediment concentrations are shown in Figures 18-20 for the 15,600-cfs base, 4,500-cfs base, and 4,500-cfs plan conditions, respectively.

40. Table 6 presents normalized shoaling results for all three channel and inflow test conditions and for the tidal and sediment conditions defined in Table 1. Ratios were based on sediment mass of predicted shoals, and express the plan condition results normalized by both base conditions. Results were rounded to two decimal places. Sediment mass gave a more reliable indicator of shoaling than shoal volume because shoal densities in the numerical model were unverified and are not expected to vary in the prototype. Annual

shoal deposits in the prototype would be thicker layers than those in the numerical model, and shoal densities would be expected to be nearly equal for similar shoaling conditions. Model shoaling predictions are for the main channel of the harbor and do not include the seaward entrance channel nor Shipyard Creek areas. However, these areas would be expected to experience similar shoaling patterns.

41. Longitudinal shoaling distributions for the verification tidal and sediment conditions and the three channel and inflow conditions are shown in Table 7. The redirection is predicted to result in a shoaling distribution which is centered farther upstream. The center of the distributions changed from river mile 14 for pre-redirection conditions to river mile 21 for base and plan conditions at 4,500-cfs inflow. Thus shoaling reductions were greater in the lower reaches of the harbor.

42. The numerical model predicted erosion for river miles 7-11. This was based on erosion of a relatively thin fluid mud layer and should not be extrapolated to deeper sediment layers, which have much greater hydraulic shear strength. However, this erosion area served as a sediment source to upstream areas in the model, and would physically offset some shoaling. Overall results were therefore not adjusted. The fluid mud modeling is described in Appendix D.

43. Table 8 shows the results of sensitivity tests of select tidal and sediment conditions. As shown, results were particularly sensitive to suspension and bed settling velocities, and to the significant erosion rate constant. Model shoaling rate decreased by about one-third between tidal cycles 2 and 4 (Table 8, last column), implying that longer, spring-to-neap tidal computations might improve model reliability.

PART V: DISCUSSION

44. Tests for 4,500-cfs base and plan shoaling were made using a number of tidal and sediment conditions, as defined in Table 1. Apparently, more than one combination of sediment characteristics would yield an acceptable verification to observed shoaling (dredging) rates. In addition, the model sensitivity to plan tests was different for different combinations of sediment characteristics. Therefore, since there were uncertainties in specifying sediment characteristics, five model predictions made with different combinations of tidal and sediment conditions were averaged. This procedure was used to test harbor deepening effects and improve the reliability of the prediction. Variability in the model prediction for a given channel and inflow condition is an indicator of the overall reliability of the prediction.

45. Table 6 presents the model test results expressed as a ratio of the sediment mass deposited in each test over the sediment mass deposited in the 15,600-cfs base test. The verification test of tidal and sediment conditions (a) resulted in a shoaling rate prediction of 0.07, or 7 percent, for the 4,500-cfs base condition, or a shoaling reduction of 93 percent. While this is about the same reduction as predicted for the 3,000-cfs inflow tests by the original physical model studies (USAEWES 1957), it is much higher than more recent predictions (Patterson 1983 and Teeter 1989). These studies are discussed in paragraphs 11 and 14, and more thoroughly in Appendix A. Because of this difference, condition (a) was not the only indicator used to predict channel deepening effects on shoaling. Four additional conditions were selected for testing and resulted in smaller ranges of shoaling reductions than condition (a). The five tidal and sediment conditions (Table 1) are representative of only partial segments within the total parameters, but cover the expected range of redirection shoaling reduction. Predictions using conditions (c) and (d) indicated a decrease in shoaling after harbor deepening which, intuitively, does not appear to be correct.

46. The pre-redirection density structure was used in condition (e); therefore this test generally had the same hydrodynamics as in the 15,600-cfs base condition. There were other parameters used in condition (e) that should have reduced the shoaling. The parameters of lower tide range, lower suspension settling coefficient, and lower critical erosion stress coefficient should have effectively reduced the shoaling according to the sensitivity

results (Table 8). Therefore, the small amount of shoaling reduction produced in condition (e) is attributed to the stratified harbor conditions imposed in the test. However, condition (e) did approximate the effects of channel deepening for pre-rediversion conditions, although the prediction of these shoaling conditions was not the focus of this study.

47. When conditions (a) through (d) are averaged, the shoaling rate ratio is about 0.32 for the 4,500-cfs base and plan tests. This relates to an average shoaling reduction of 68 percent, which is reasonably close to the reduction predicted by the sediment budget method described in Appendix A.

48. Since the purpose of this study was to provide disposal site capacity requirements, a conservative approach was used by taking the larger numbers of the predicted range. Another reason for the conservative approach was the lack of site-specific sediment information. The maximum shoaling increase for conditions (a) through (d) between the 4,500-cfs base and 4,500-cfs plan tests was 0.04 relative to the 15,600-cfs shoaling rate, and is another conservative indicator of shoaling increase due to channel deepening. The mean and standard deviation for the 4,500-cfs base-to-plan shoaling differences relative to the 15,600-cfs shoaling rate for conditions (a) through (d) was 0.00 and 0.04, respectively. The mean incremented by the standard deviation represents another measure of the upper predictive range. Therefore, the conservative model prediction for increased shoaling due to channel deepening is 0.04 times the shoaling rate of the 15,600-cfs base condition or 0.15 times the shoaling rate of the 4,500-cfs base condition, and is summarized in the next section.

PART VI: CONCLUSIONS

49. Harbor deepening to -40 ft mlw was predicted to increase harbor dredging requirements by about 15 percent for rediversion conditions, or 210,000 cu yd annually at 4,500 cfs. The rediversion channel deepening effect was the main focus of this study, and the increased shoaling will amount to about 4 percent of the pre-rediversion condition. The following tabulation summarizes the combined results for all three channel and inflow conditions.

Average Inflow cfs	Charleston Harbor Dredging Requirement, 10 ⁶ cu yd per year,* for Channel Depth, ft mlw	
	-35	-40
	15,600	4.81**
4,500	1.43††	1.64‡
3,000	1.27††	1.46‡

* Excluding entrance channel dredging.

** Prototype average for 1965-1984.

† Prediction based on shoaling rate ratio for tidal and sediment condition (e) which had stratification and density currents as for 15,600-cfs base. See Tables 4 and 6, and paragraph 46.

†† Prediction based on sediment budget analysis. See Appendix A.

‡ Prediction based on channel deepening effects from schematic numerical model. See Table 6 and paragraph 48.

50. Entrance channel shoaling was not predicted. However, no increase in shoaling is expected as a result of the harbor channel deepening in the entrance channel based on extrapolation of model shoaling distributions.

51. The centroid of the shoaling distribution is expected to move about 7 miles upstream as a result of rediversion of the Cooper River. Numerical model results indicated that the harbor channel from river mile 7 to 11 will be self-maintaining after rediversion and channel deepening.

52. Numerical modeling of fine-grained sediment transport in estuaries

is not a simple matter. The model did not respond in a simple way to changes in channel depth. Results depended in a complex way on other tidal and sediment conditions imposed. Therefore, numerical hydrodynamic and sediment models do not lend themselves to simplified application to these types of problems. In this study, sensitivity testing was used to examine a range of possible effects, and a value at the conservative end of the range selected to characterize the response.

REFERENCES

- Ariathurai, R., MacArthur, R. C., and Krone, R. B. 1977. "Mathematical Model of Estuarine Sediment Transport," Technical Report D-77-12, US Army Engineer Waterways Experiment Station, Vicksburg, MS.
- Benson, H. A. 1976. "Effects of 40-ft Charleston Harbor Project on Tides, Currents, and Salinities," Miscellaneous Paper HL-76-9, US Army Engineer Waterways Experiment Station, Vicksburg, MS.
- Blumberg, A. F. 1977 (Mar). "Numerical Models of Estuarine Circulation," Journal of the Hydraulics Division, American Society of Civil Engineers, Vol 103, No. HY3, pp 295-310.
- Blumberg, A. F., and Kantha, L. H. 1985. "Open Boundary Condition for Circulation Models," Journal of the Hydraulics Division, American Society of Civil Engineers, Vol 111, No. 2, pp 237-255.
- Committee on Tidal Hydraulics, Corps of Engineers, US Army. 1966. "Charleston Harbor, South Carolina: A Review of Certain Aspects of Plans for Rediverting Santee-Cooper Power Plant Discharges from Cooper River," US Army Engineer Waterways Experiment Station, Vicksburg, MS.
- Finlayson, B. A. 1972. The Method of Weighted Residuals and Variational Principles, Academic Press, New York.
- Hunt, J. R. 1982. "Self-Similar Particle Size Distributions During Coagulation: Theory and Experimental Verification," Journal of Fluid Mechanics, Vol 122, pp 169-185.
- Hunt, S. D. 1981. "A Comparative Review of Laboratory Data on Erosion of Cohesive Sediment Beds," UFL/COEL/MP-81/7, Coastal and Oceanographic Engineering Department, University of Florida, Gainesville, FL.
- Krone, R. B. 1962. "Flume Studies of the Transport of Sediment in Estuarial Shoaling Processes, Final Report," Hydraulic Engineering Laboratory and Sanitary Engineering Research Laboratory, University of California, Berkeley, CA.
- Krone, R. B. 1963. "A Study of Rheological Properties of Estuarial Sediment," Technical Bulletin No. 7, Committee on Tidal Hydraulics, Corps of Engineers, US Army; prepared by US Army Engineer Waterways Experiment Station, Vicksburg, MS.
- Kuenen, P. H. 1968 (Sep). "Settling Convection and Grain-size Analysis," Journal of Sedimentary Petrology, Vol 38, No. 3, pp 817-831.
- Kynch, G. J. 1952. "A Theory of Sedimentation," Faraday Society Transactions, Vol 48, pp 166-176.
- Mehta, A. J., Hayter, E. J., Parker, W. R., and Teeter, A. M. 1986. "Cohesive Sediment Transport Processes," Proceedings, Sedimentation Control Committee, National Research Council, Washington, DC.
- Munk, W. H., and Anderson, E. R. 1948. "A Note on the Theory of the Thermocline," Journal of Marine Research, Vol 26, pp 24-33.
- Owen, M. W., 1970 (Dec). "Properties of a Consolidating Mud," Report No. INT 83, Hydraulic Research Station, Wallingford, England.
- Parsons, T., and Takahashi, M. 1973. Biological Oceanographic Processes, Pergamon Press, Elmsford, NY.

- Partheniades, E. 1962. "A Study of Erosion and Deposition of Cohesive Soils in Salt Water," Ph.D. dissertation, University of California, Berkeley, CA.
- Patterson, G. G. 1983. "Effect of the Proposed Cooper River Rediversion on Sedimentation in Charleston Harbor, South Carolina," Water-Resources Report 83-4198, US Geological Survey, Columbia, SC.
- Richardson, J. F., and Zaki, W. N. 1954. "The Sedimentation of a Suspension of Uniform Spheres under Conditions of Viscous Flow," Chemical Engineering Science, Vol 3, pp 65-73.
- Sheng, Y. P. 1983. "Mathematical Modeling of Three-Dimensional Coastal Currents and Sediment Dispersion: Model Development and Application," Technical Report CERC-83-2, US Army Engineer Waterways Experiment Station, Vicksburg, MS.
- Smith, T. J. 1982. "On the Representation of Reynolds Stress in Estuaries and Shallow Coastal Seas," Journal of Phys. Oceano., Am. Meteor. Soc., Vol. 12, pp. 914-921.
- Smith, T. J., and H. S. Takhar. 1979. "On the Calculation of Width Averaged Flow Due to Long Waves in an Open Channel," Journal of Hyd. Res., Vol. 17, pp. 329-340.
- Teeter, A. M. 1986. "Vertical Transport in Fine-Grained Suspensions and Newly Deposited Sediment," in Estuarine Cohesive Sediment Dynamics, A. J. Mehta Ed., Lecture Notes on Coastal and Estuarine Studies No. 14, Springer-Verlag, New York.
- Teeter, A. M. 1987. "Alcatraz Disposal Site Investigation- Report 3- San Francisco Bay-Alcatraz Disposal Site Erodibility," Misc. Paper HL-86-1, US Army Engineer Waterways Experiment Station, Vicksburg, Miss.
- Teeter, A. M. 1989. "Effects of Cooper River Rediversion Flows on Shoaling Conditions in Charleston Harbor, Charleston, South Carolina," Tech. Rpt. HL-89-3, US Army Engineer Waterways Experiment Station, Vicksburg, Miss.
- US Army Engineer District, Charleston. 1954. "Investigation for Reduction of Maintenance Dredging in Charleston Harbor, S.C.; Part 2, Materials Testing Laboratory Investigation of Properties of Shoals and Materials in Movement," Charleston, SC.
- US Army Engineer District, Charleston. 1966 (Apr). "Spoil Disposal Study-Charleston Harbor, S.C.," Charleston, SC.
- US Army Engineer Waterways Experiment Station. 1957. "Investigation for Reduction of Maintenance Dredging in Charleston Harbor, South Carolina," Technical Report No. 2-444, U.S. Army Engineer Waterways Experiment Station, Vicksburg, Miss.
- Wang, D.-P. 1983. "Two-Dimensional Branching Salt Intrusion Model," Journal of Water., Port, Coastal, and Ocean Eng., ASCE, Vol. 109, No.1, February, 1983, pp 103-112.
- Wang, D.-P. 1984. "Mutual Intrusion of a Gravity Current and Density Front Formation," Journal of Phys. Oceano., Am. Meteor. Soc., Vol. 14, pp. 1191-1199.

Table 1
Tidal and Sediment Conditions

<u>Tide and Sediment Condition</u>	<u>Tidal and Sediment Condition Designation</u>				
	<u>(a)*</u>	<u>(b)</u>	<u>(c)</u>	<u>(d)</u>	<u>(e)</u>
Tide Range at Ocean, m	1.70	1.70	1.70	1.70	1.60
Salinity Distribution	Normal	Normal	Normal	Normal	15,600-cfs base
Suspension Settling Coefficient A_1 ($W_s = A_1 C^{4/3}$)	1.1E-7	1.4E-7	1.6E-7	1.8E-7	1.0E-7
Critical Stress for Deposition τ_{cd} , N/sq m	0.06	0.08	0.08	0.08	0.08
Fluid Mud Settling Coefficient W_1 , cm/sec ($W_h = W_1 \cdot f(C_s)$)	1E-4	1E-4	5E-5	1E-5	1E-4
Critical Erosion Stress Coefficient D_{h1} , ($\tau_{ch} = D_{h1} \cdot C_s^{5/2}$)	90	90	90	90	40
No. of Depositional Tidal Cycles (step 3)	2	4	2	2	2

* Verification condition.

Table 2
Tidal Verification for 15,600-cfs Base Condition

<u>River Mile</u>	<u>Node</u>	<u>Model Tide Range, m</u>		<u>Model Average Phase, hr</u>	
		<u>Physical</u>	<u>Numerical</u>	<u>Physical</u>	<u>Numerical</u>
1	1	1.52	1.73	0	0
9	11	1.80	1.81	0.4	0.3
19	21	1.86	1.87	1.2	1.0
25	27	1.80	1.91	1.5	1.3
33	31	1.68	1.67	2.3	2.0
41	35	1.13	1.64	3.2	2.5
45	37	0.64	1.17	4.1	3.3
51	40	0.55	1.12	5.0	3.7

Table 3
Tidal Verification for 4,500-cfs* Base Condition

<u>River Mile</u>	<u>Node</u>	<u>Model Tide Range, m</u>		<u>Model Average Phase, hr</u>	
		<u>Physical</u>	<u>Numerical</u>	<u>Physical</u>	<u>Numerical</u>
1	1	1.68	1.71	0	0
9	11	1.83	1.71	0.3	0.5
19	21	1.80	1.64	1.1	1.5
25	27	1.74	1.66	1.4	1.5
33	31	1.68	1.45	2.1	2.5
41	35	1.55	1.38	3.0	3.0
45	37	0.94	1.12	3.9	3.5
51	40	0.94	1.00	4.1	4.0

* Physical model had 3,500-cfs inflow.

Table 4
Tidal Comparison for 4,500-cfs* Plan Condition

<u>River Mile</u>	<u>Node</u>	<u>Model Tide Range, m</u>		<u>Model Average Phase, hr</u>	
		<u>Physical</u>	<u>Numerical</u>	<u>Physical</u>	<u>Numerical</u>
1	1	1.65	1.72	0.0	0.0
9	11	1.86	1.76	0.3	0.3
19	21	1.86	1.79	0.9	1.0
25	27	1.83	1.81	1.3	1.5
33	31	1.68	1.55	2.0	2.2
41	35	1.55	1.51	3.0	2.7
45	37	0.91	1.19	3.7	3.5
51	40	0.98	1.08	4.1	4.0

* Physical model had 3,500-cfs inflow.

Table 5
Shoaling Verification for 15,600-cfs Base Condition

<u>River Mile After</u> <u>River Mile</u>	<u>Node</u>	<u>Prototype Dredged Volumes</u>		<u>Verification</u>	<u>Shoal/</u> <u>Reach</u>
		<u>1,000 cu yd/year</u>	<u>cu m/cycle</u>	<u>Dredged Volumes*</u> <u>cu m/cycle</u>	
6	8	315	319	901	Anchorage
7	9	452	458	479	Anchorage
8	10	0	0	223	--
9	11	713	723	10	Tidewater, 6A,6C
10	12	620	628	15	6A,6C
11	13	134	136	223	6A,6B,6
12	14	58	59	261	6B,6
13	15	360**	365**	233	5A
14	16	46	47	209	5A
15	17	0	0	189	--
16	18	170	172	177	4
17	19	9	9	173	3
18	20	48	49	220	1&2,3
19	21	200	203	301	1&2
20	22	120	122	370	1&2, NAD
21	23	400	405	303	NAD
22	24	378	383	83	NAD
23	25	10	20	5	NAD
TOTAL		4,145	4,088	4,374 [†]	

* Dredged volumes = 1.28 times shoaling volumes, assuming 22 percent runback.

** Excluding Shipyard River which amounts to 780,000 cu yd annually.

† On average, Cs = 0.334 g/cu cm.

Table 6
Shoaling Test Results

Tidal and** Sediment Condition	Shoaling Rate Ratio* for Channel and Inflow Condition			Relative to 4,500-cfs Base
	Relative to 15,600-cfs Base			
	15,600-cfs Base	4,500-cfs Base	4,500-cfs Plan	4,500-cfs Plan
(a)	1.0	0.07	0.09	1.33
(b)		0.17	0.21	1.22
(c)		0.42	0.41	0.97
(d)		0.62	0.57	0.91
(e)		0.70	0.93	1.32
Averages:		0.40	0.44	1.15
Standard Deviations:		0.28	0.33	0.20

* Ratio = $\frac{\text{mass of sediment deposited}}{\text{mass of sediment deposited in base test}}$

** See paragraph 40 in text and Table 1 for explanation.

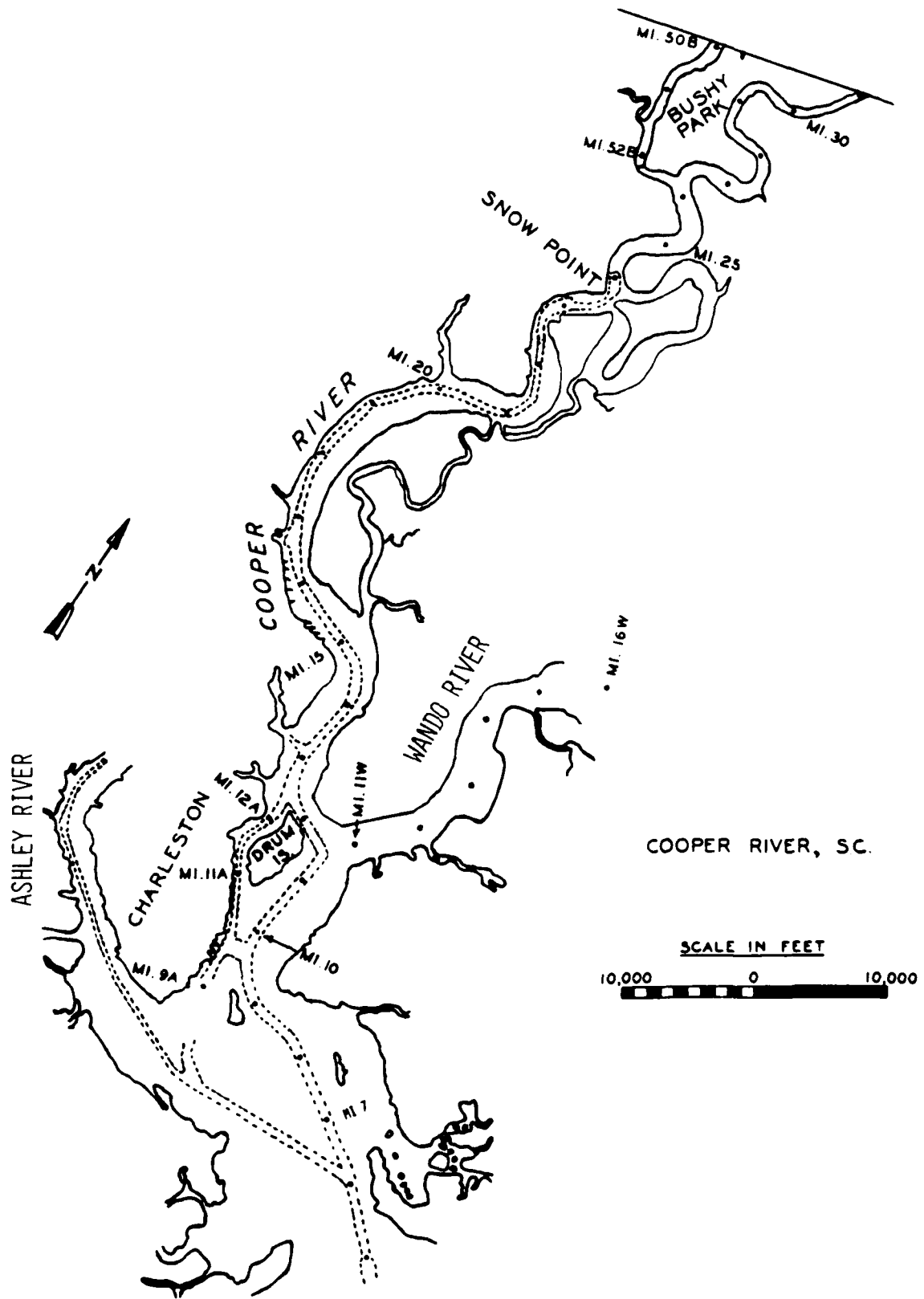
Table 7
Model Shoaling Distributions

Mile After		Model Shoaling Distributions for Verification Conditions Metric Tons per Tidal Cycle		
River Mile	Node	15,600-cfs Base	4,500-cfs Base	4,500-cfs Plan
6	8	172	5	8
7	9	109	-5	-1
8	10	68	-10	-6
9	11	35	-15	-9
10	12	30	-14	-10
11	13	55	-4	-4
12	14	60	0	0
13	15	56	4	3
14	16	53	7	7
15	17	50	8	8
16	18	48	6	6
17	19	47	7	8
18	20	57	11	12
19	21	71	14	13
20	22	83	15	14
21	23	79	17	16
22	24	49	20	21
23	25	<u>21</u>	<u>19</u>	<u>28</u>
TOTAL		1,142	84	122

Table 8

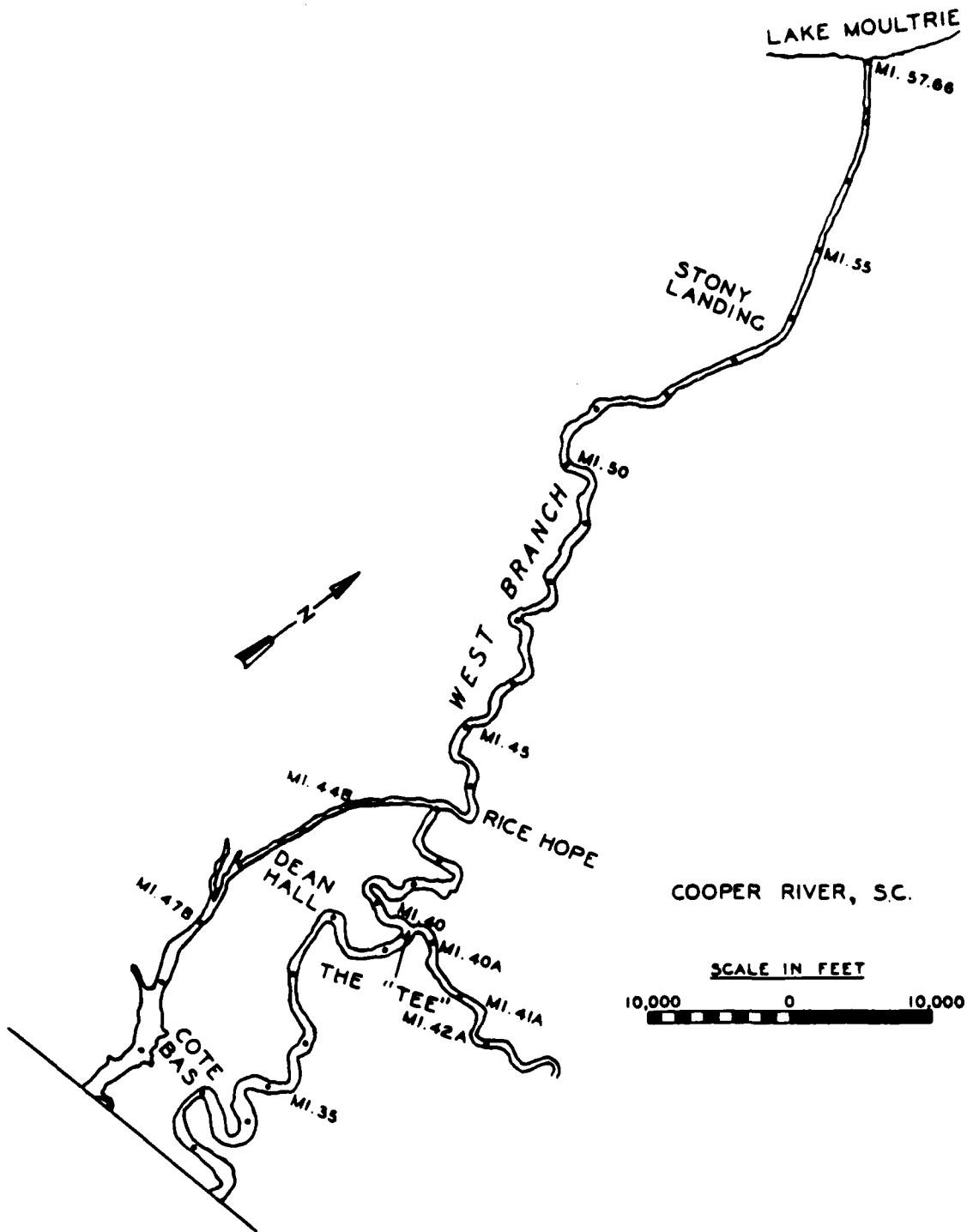
Sensitivity Tests

<u>Tide and Sediment Condition</u>	<u>Channel and Inflow Condition</u>			
	<u>Base</u>	<u>15,600-cfs</u> <u>Base</u>	<u>Base</u>	<u>4,500-cfs</u> <u>Base</u>
Tide Range at Ocean, m	<u>1.70 & 1.60</u>	1.70	1.70	1.70
Salinity Distribution	Normal	Normal	Normal	Normal
Suspension Settling Coefficient A_1 ($W_s = A_1 C^{4/3}$)	1.0E-7	<u>1.0E-7 & 2.0E-7</u>	1.0E-7	1.6E-7
Critical Stress for Deposition τ_{cd} , N/sq m	0.08	0.08	<u>0.08 & 0.05</u>	0.08
Fluid Mud Settling Coefficient W_l , cm/sec ($W_h = W_l \cdot f(C_g)$)	1E-4	1E-4	1E-4	1E-4
Critical Erosion Stress Coefficient Dh_1 , ($\tau_{ch} = Dh_1 \cdot C_g^{5/2}$)	40	40	40	90
No. of Depositional Tidal Cycles	2	2	2	<u>2 & 4</u>
Shoaling rate m. tons per cycle	924 & 361	924 & 3,947	924 & 863	480 & 8,447 305 & 193



a. Charleston Harbor and the lower Cooper River Estuary

Figure 1. Location map (Continued)



b. Upper Cooper River Estuary

Figure 1. (Concluded)

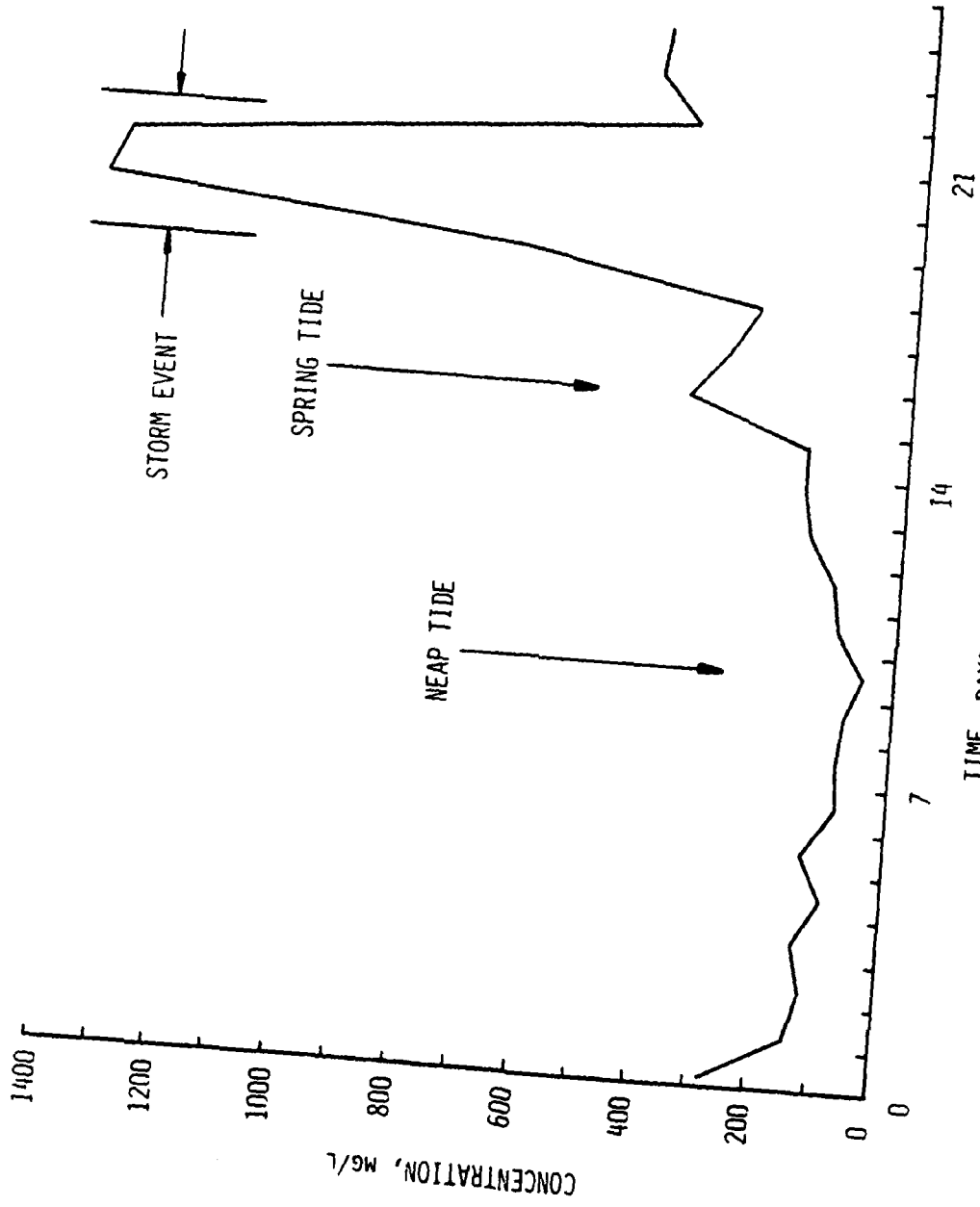
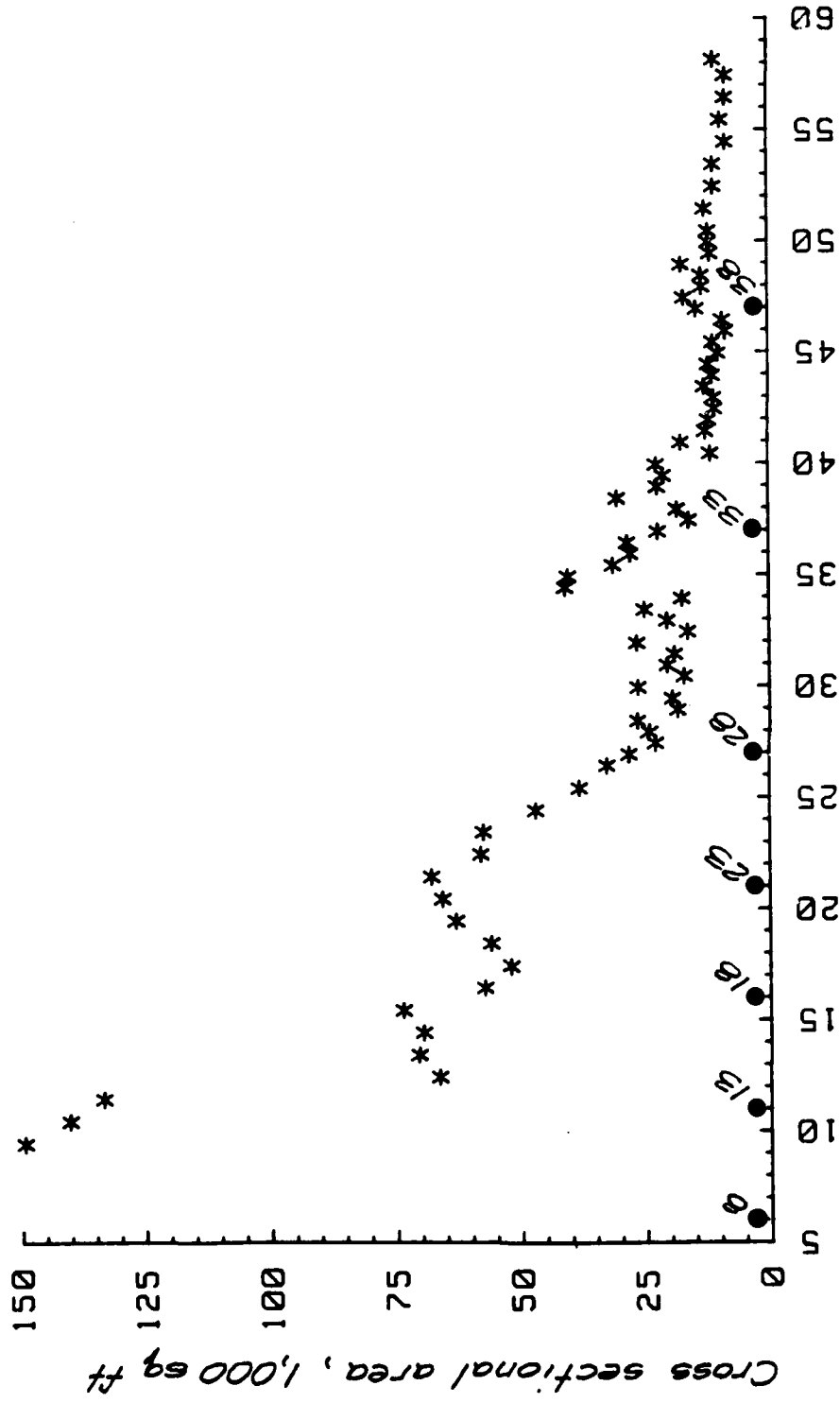


Figure 2. Daily tidal-averaged suspended sediment concentration at river mile 8.0, 0.75 depth



River miles and node numbers (•)

Figure 3. Cross-sectional areas along the Cooper River estuary

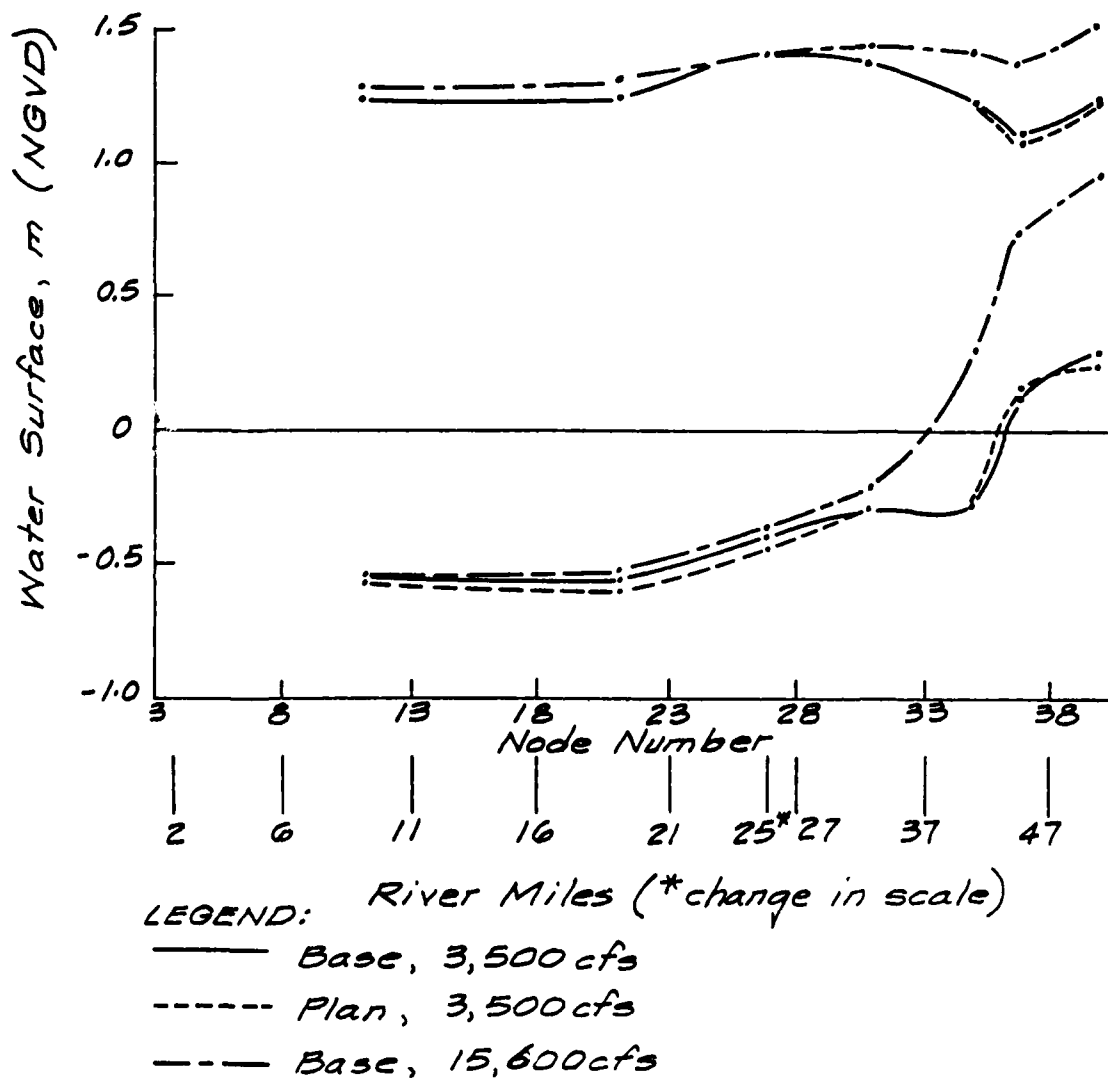


Figure 4. Physical model tidal envelopes (data from Benson 1976)

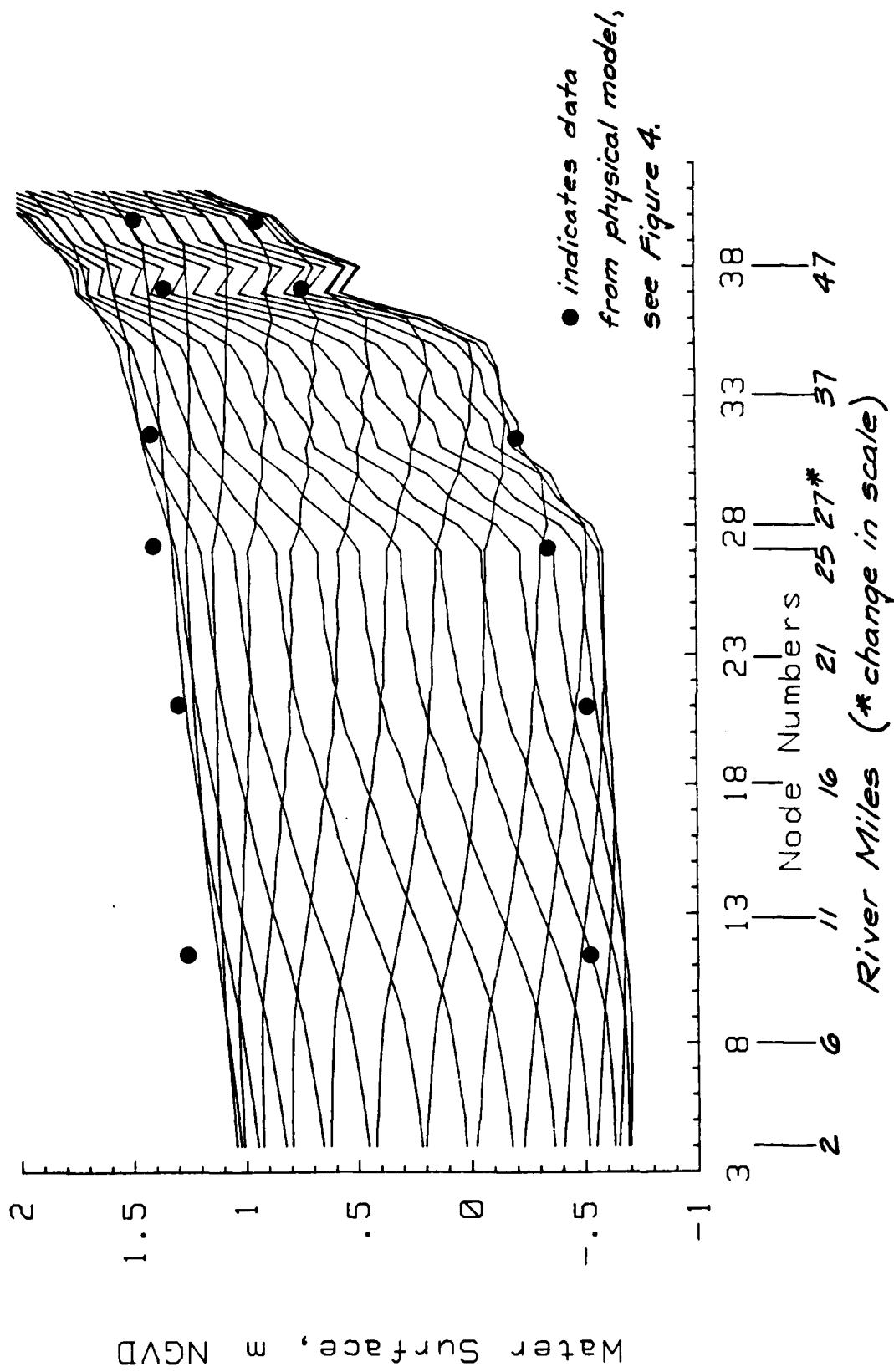


Figure 5. Water-surface profiles at half-hourly intervals for 15,600-cfs base test

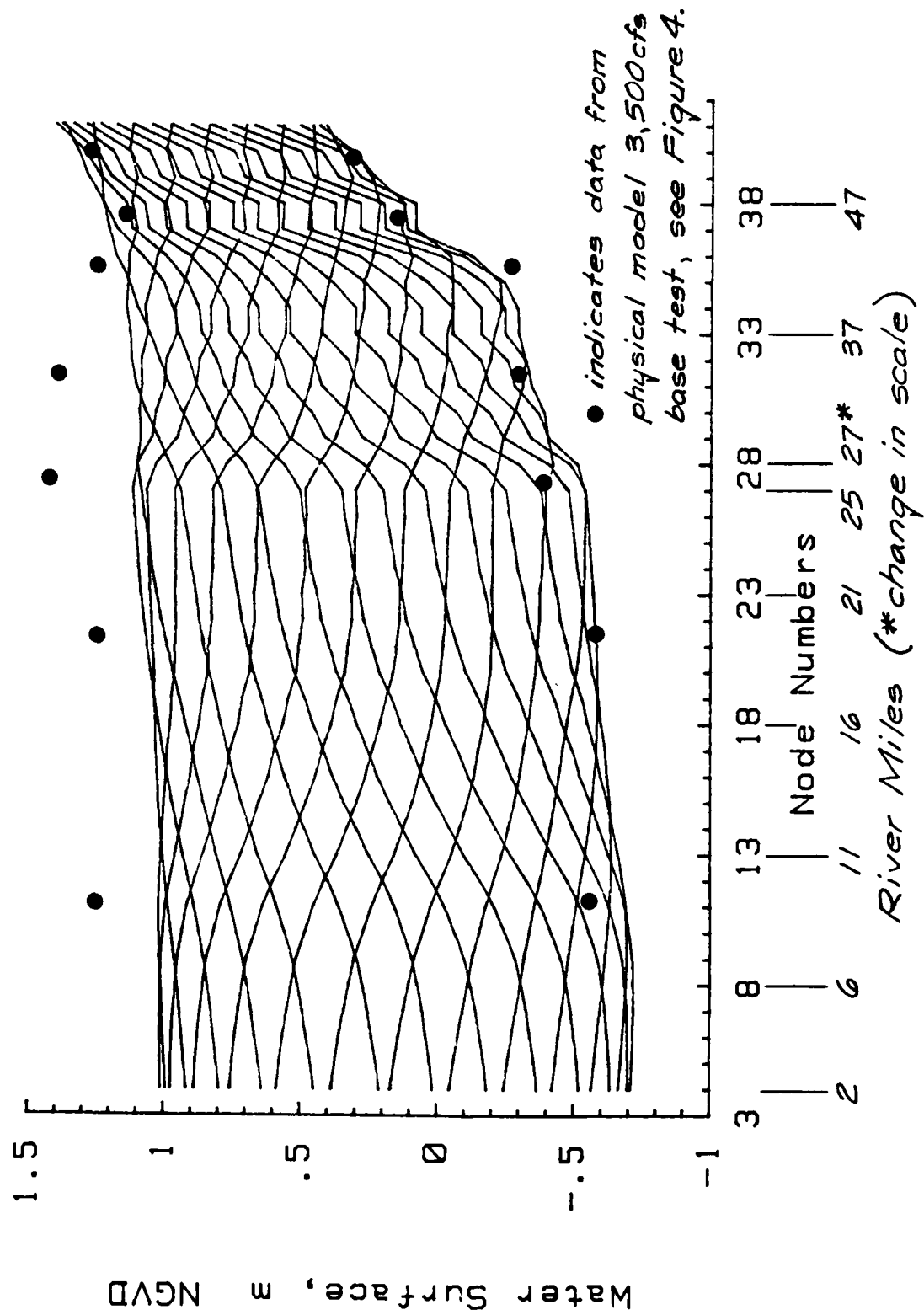


Figure 6. Water-surface profiles at half-hourly intervals for 4,500-cfs base test

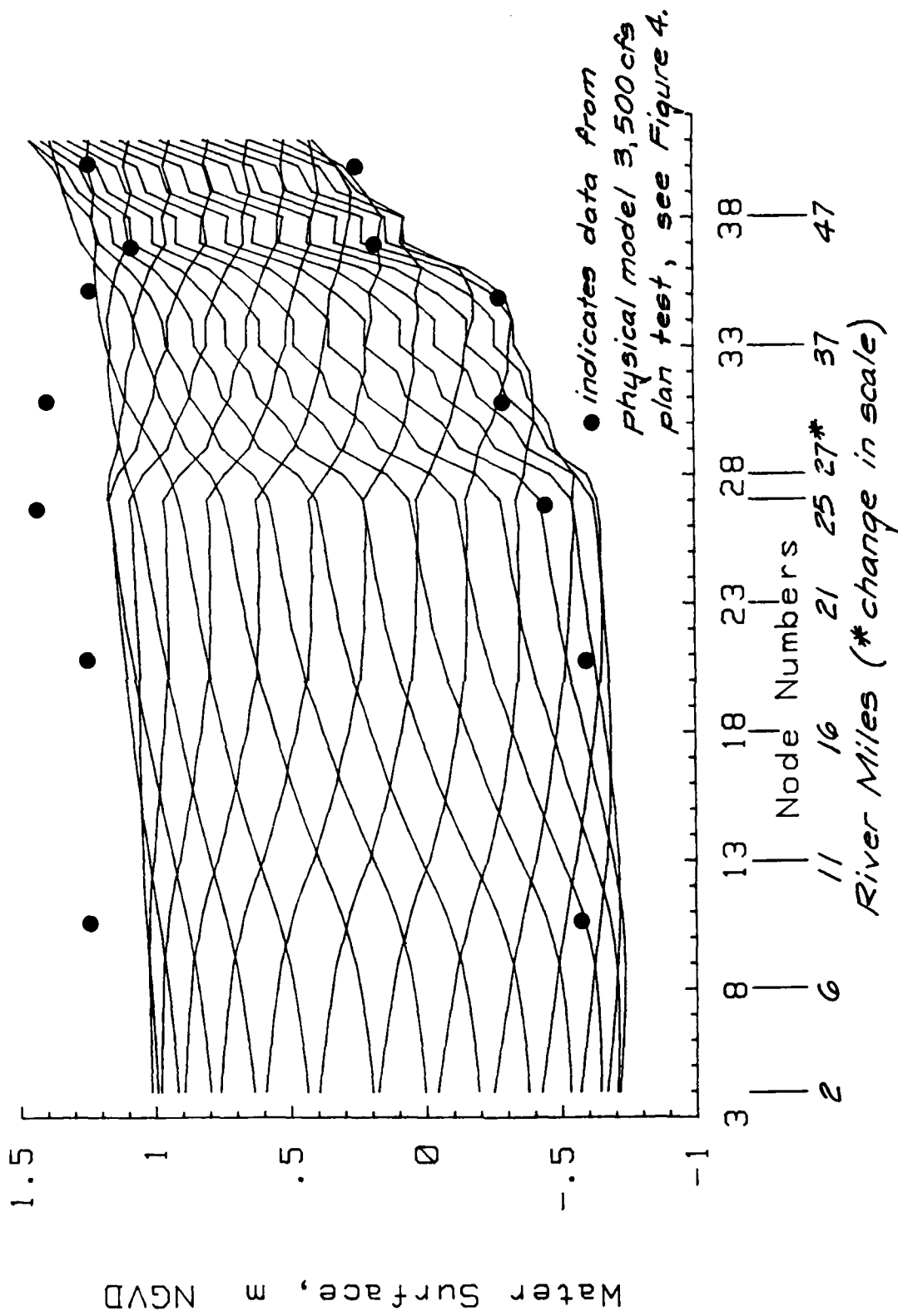
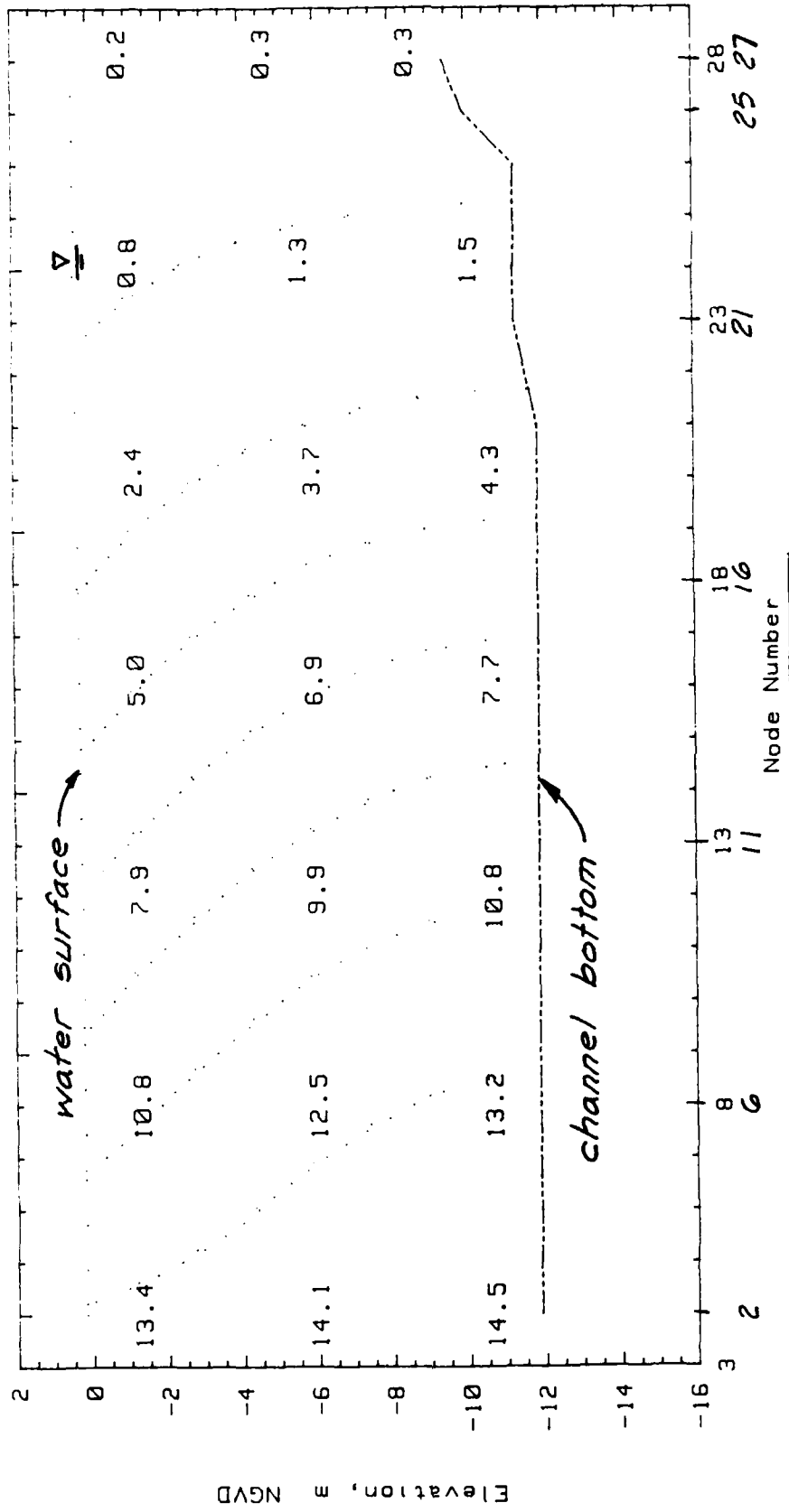


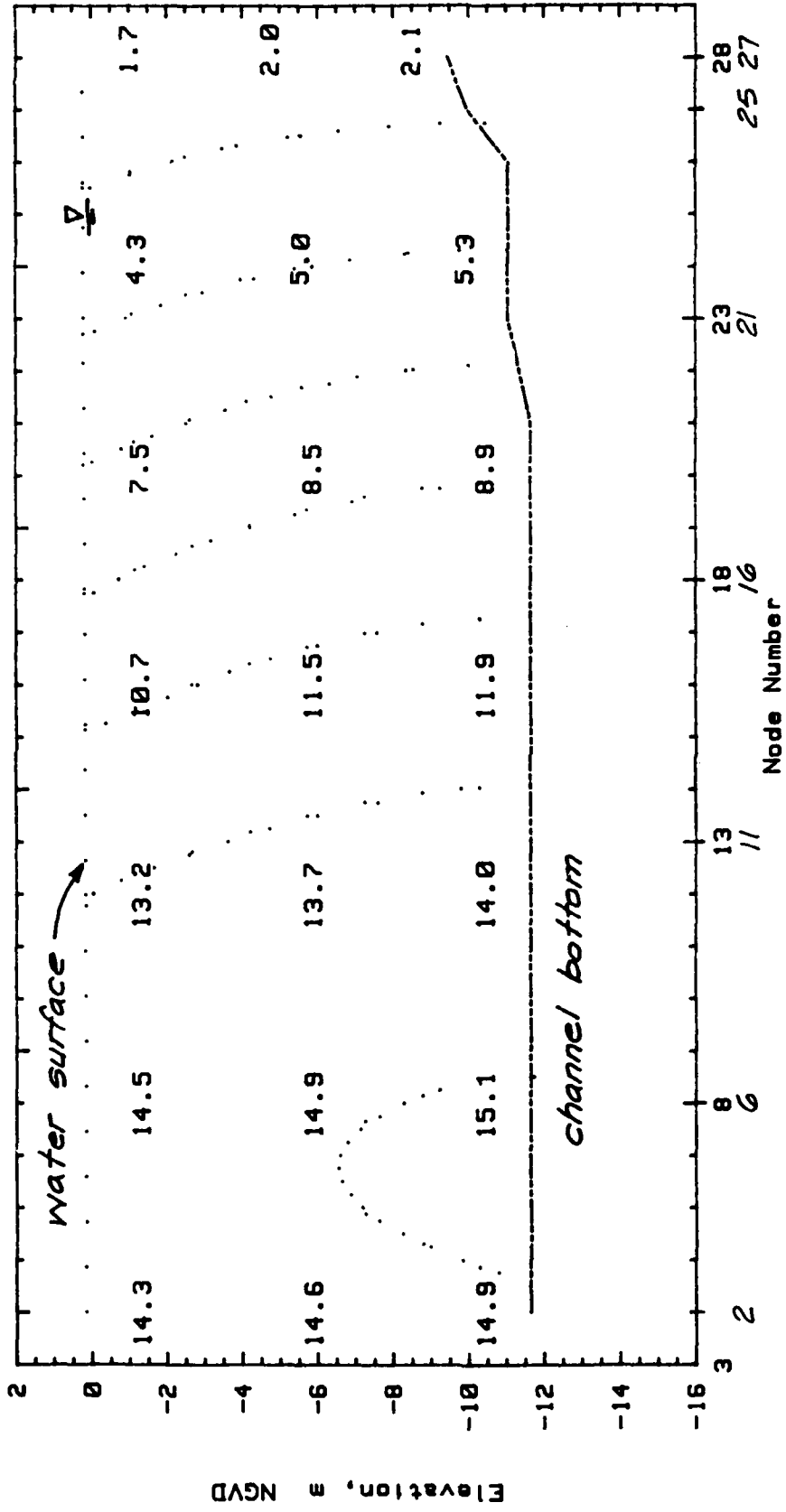
Figure 7. Water-surface profiles at half-hourly intervals for 4,500-cfs plan test



NOTE: CHLORINITIES IN PPT
 CONTOUR INTERVAL 2 PPT

GEOMETRIC DISTORTION-1207:1

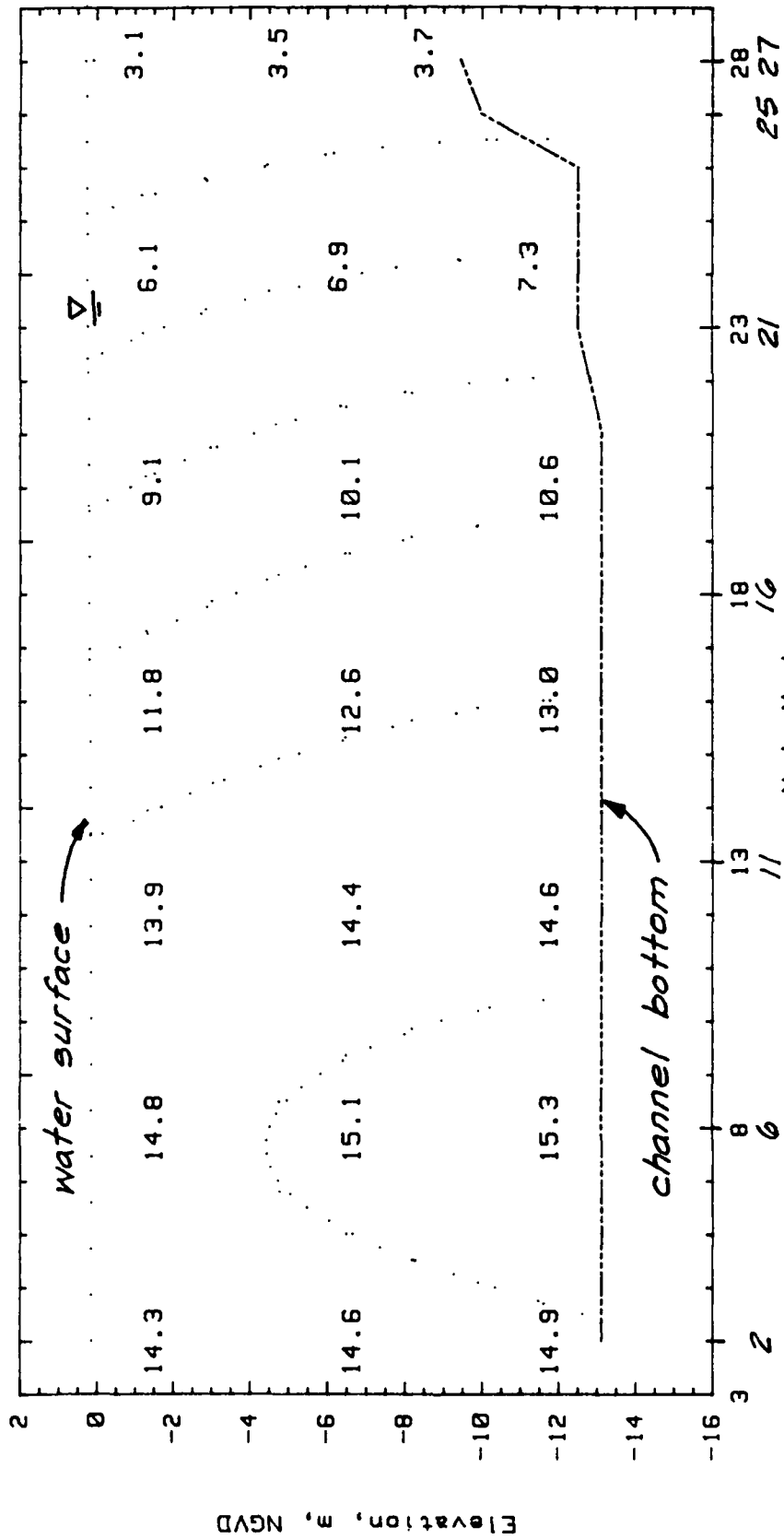
Figure 8. Profile of chlorinity values along the harbor channel for 15,000-cfs base test



NOTE: CHLORINITIES IN PPT
 CONTOUR INTERVAL 2 PPT

GEOMETRIC DISTORTION-1207:1

Figure 9. Profile of chlorinity values along the harbor channel for 4,500-cfs base test



NOTE: CHLORINITIES IN PPT
 CONTOUR INTERVAL 2 PPT

Node Number

River Miles

GEOMETRIC DISTORTION-1207:1

Figure 10. Profile of chlorinity values along the harbor channel for 4,500-cfs plan test

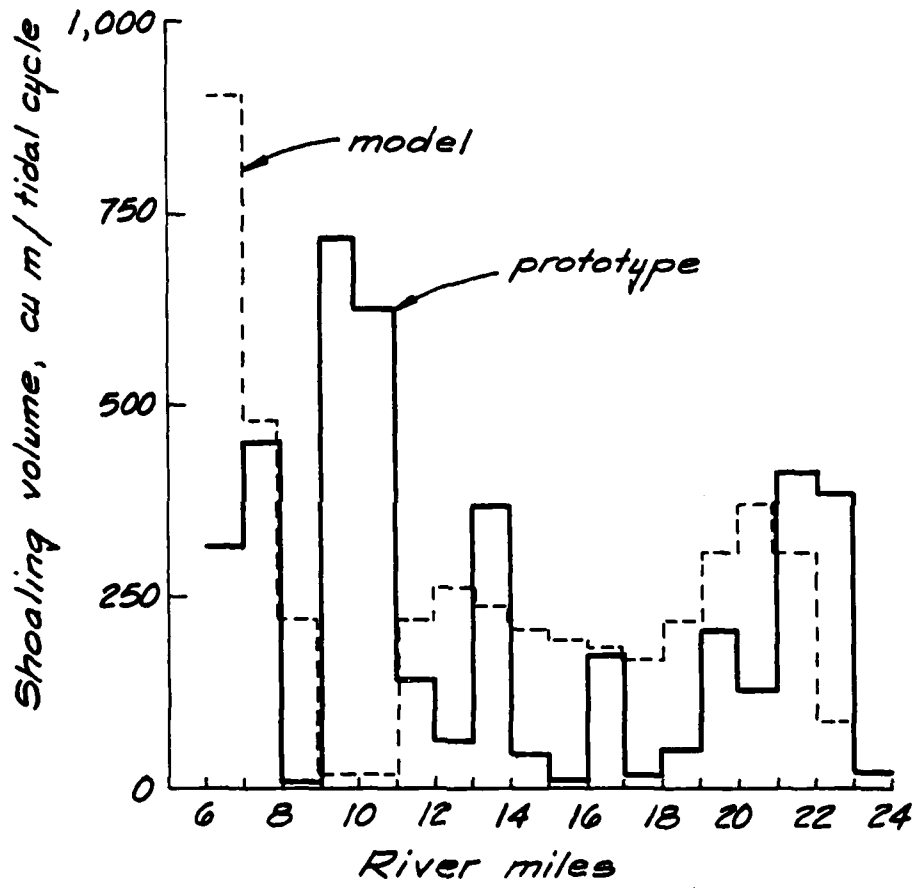


Figure 11. Verification shoaling distribution for 15,600-cfs base condition

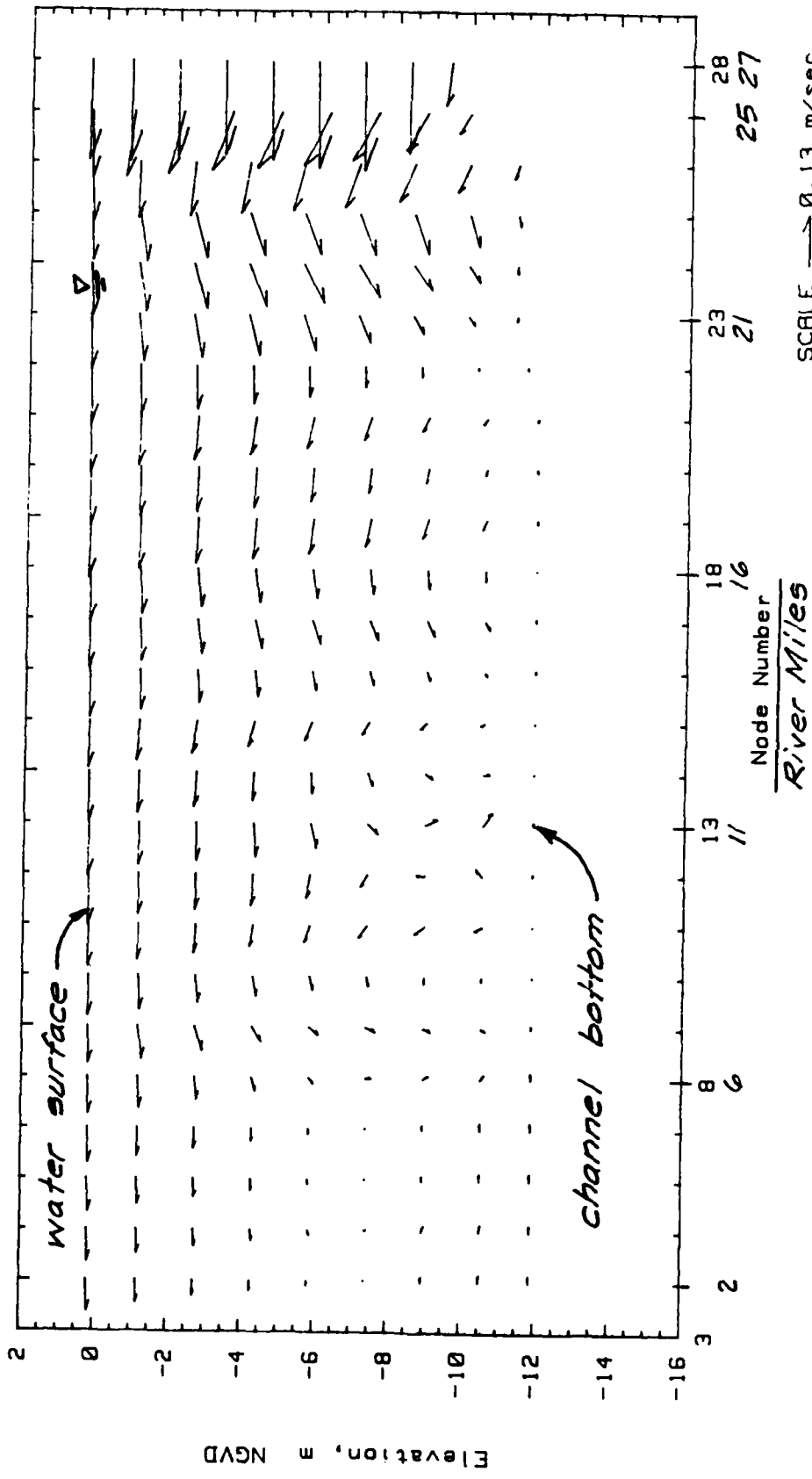


Figure 12. Profile of vertical circulation vectors along the harbor channel for 15,000-cfs base test

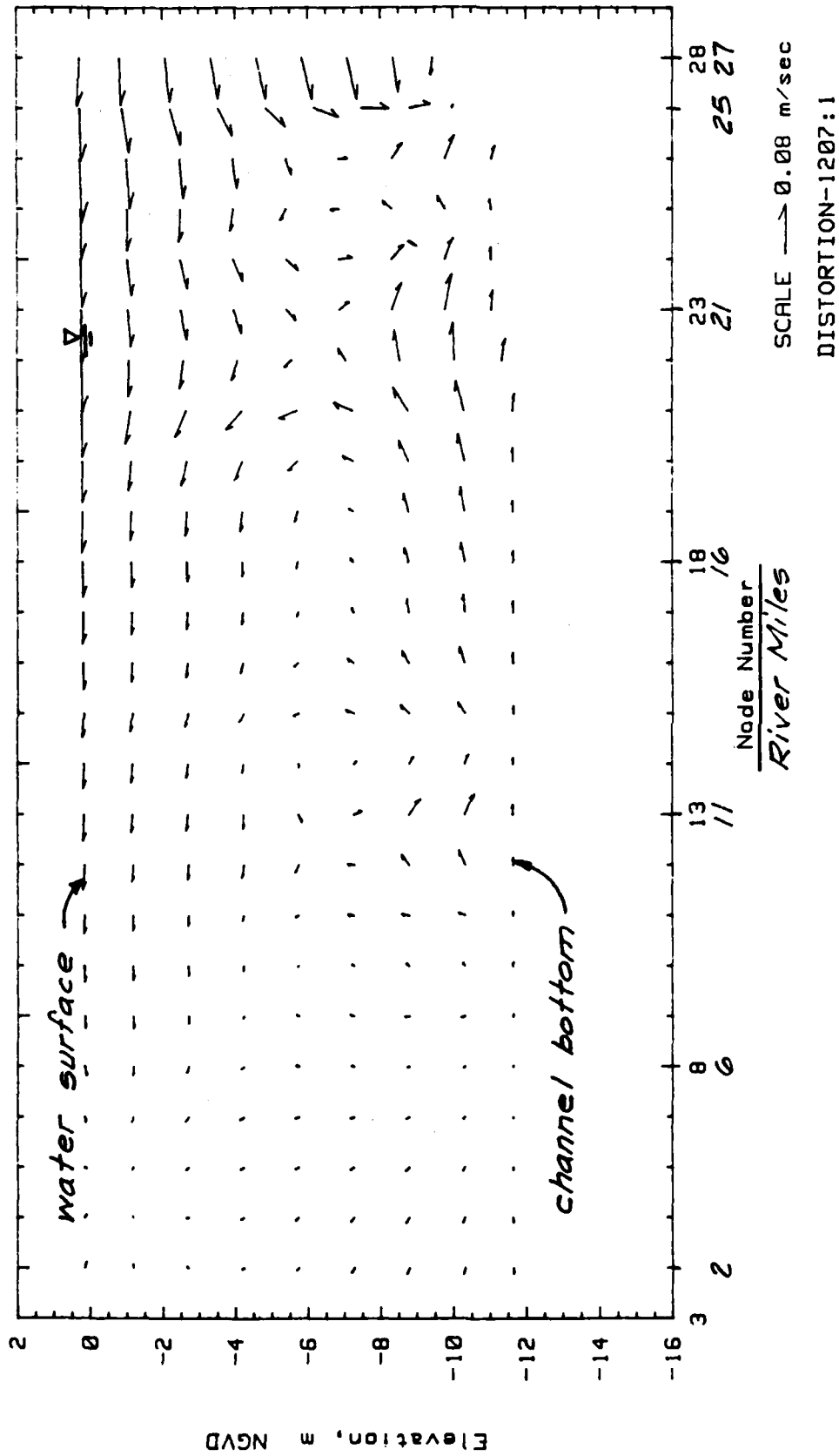


Figure 13. Profile of vertical circulation vectors along the harbor channel for 4,500-cfs base test

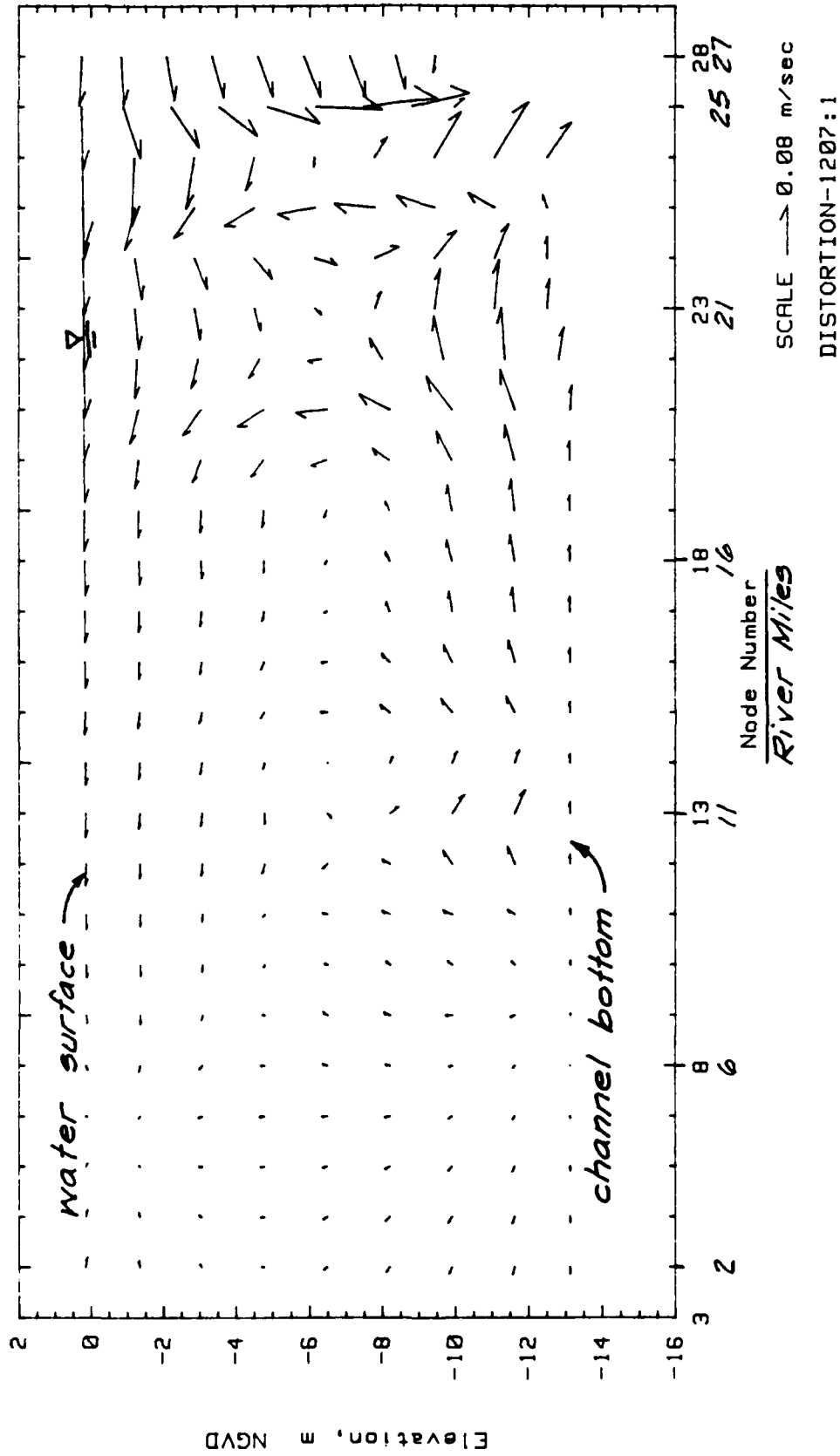


Figure 14. Profile of vertical circulation vectors along the harbor channel for 4,500-cfs plan test DISTORTION-1207:1

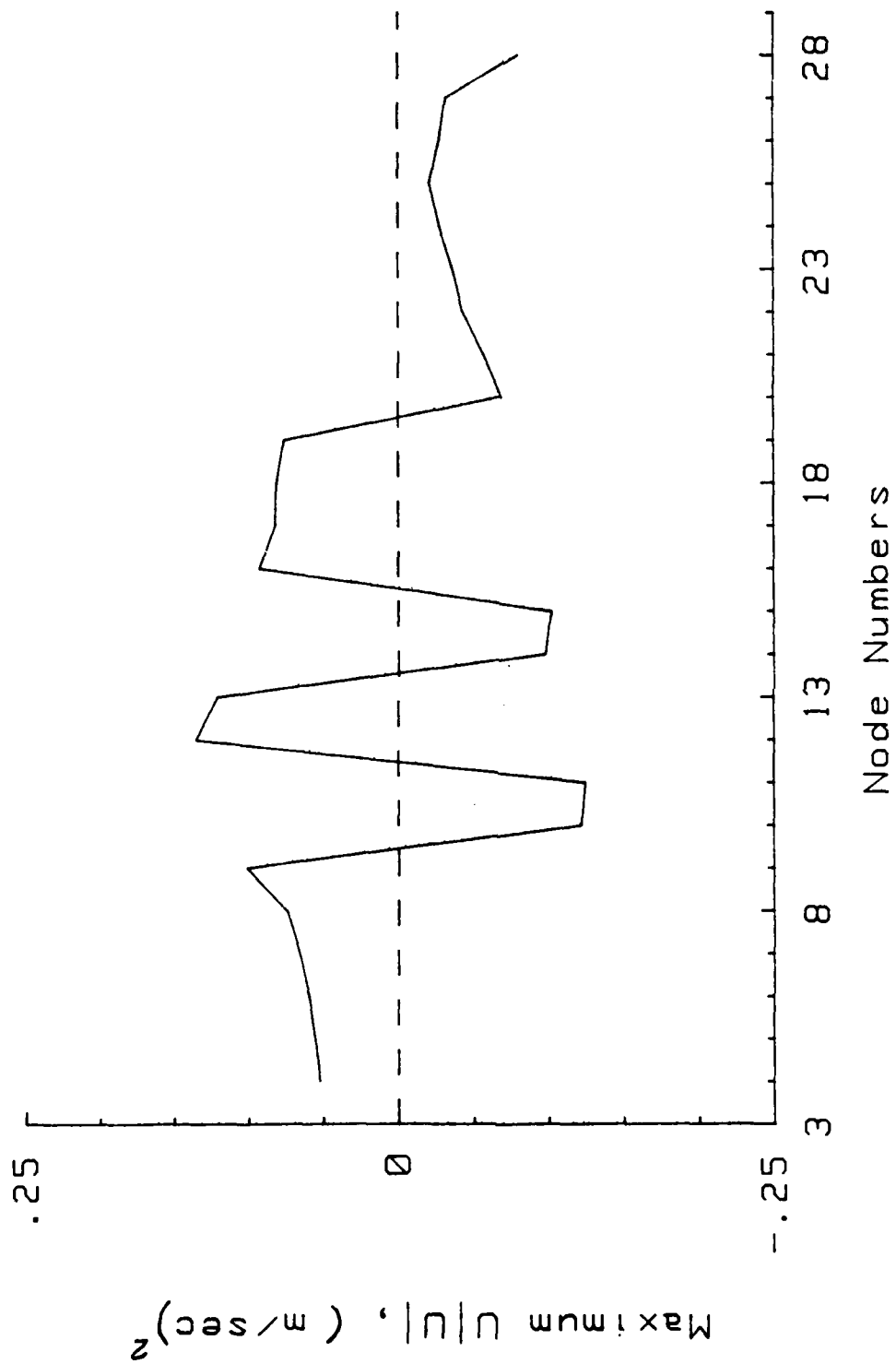


Figure 15. Maximum near-bed velocities squared and directions along the harbor channel for 15,600-cfs base test

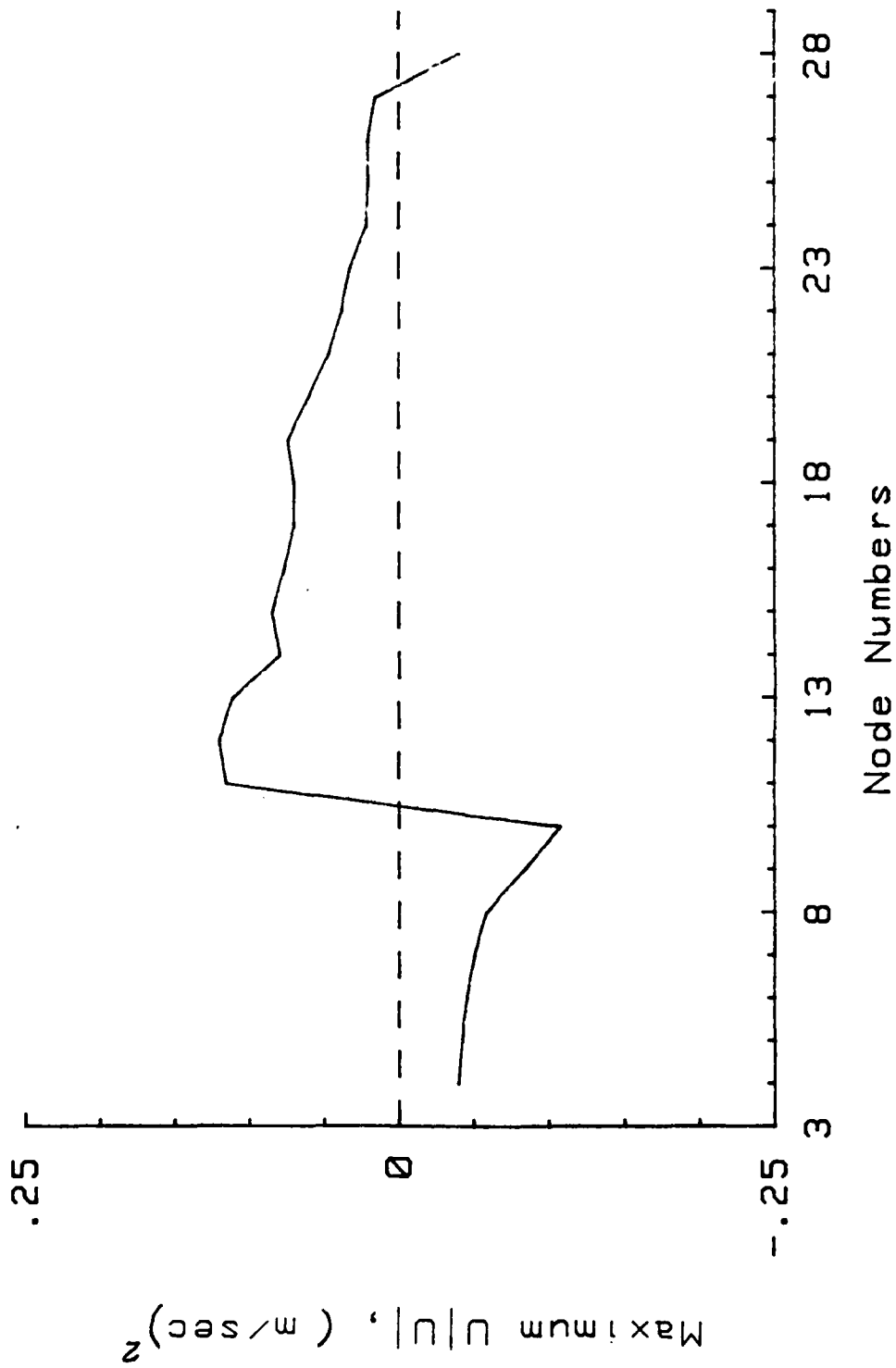


Figure 16. Maximum near-bed velocities squared and directions along the harbor channel for 4,500-cfs base test

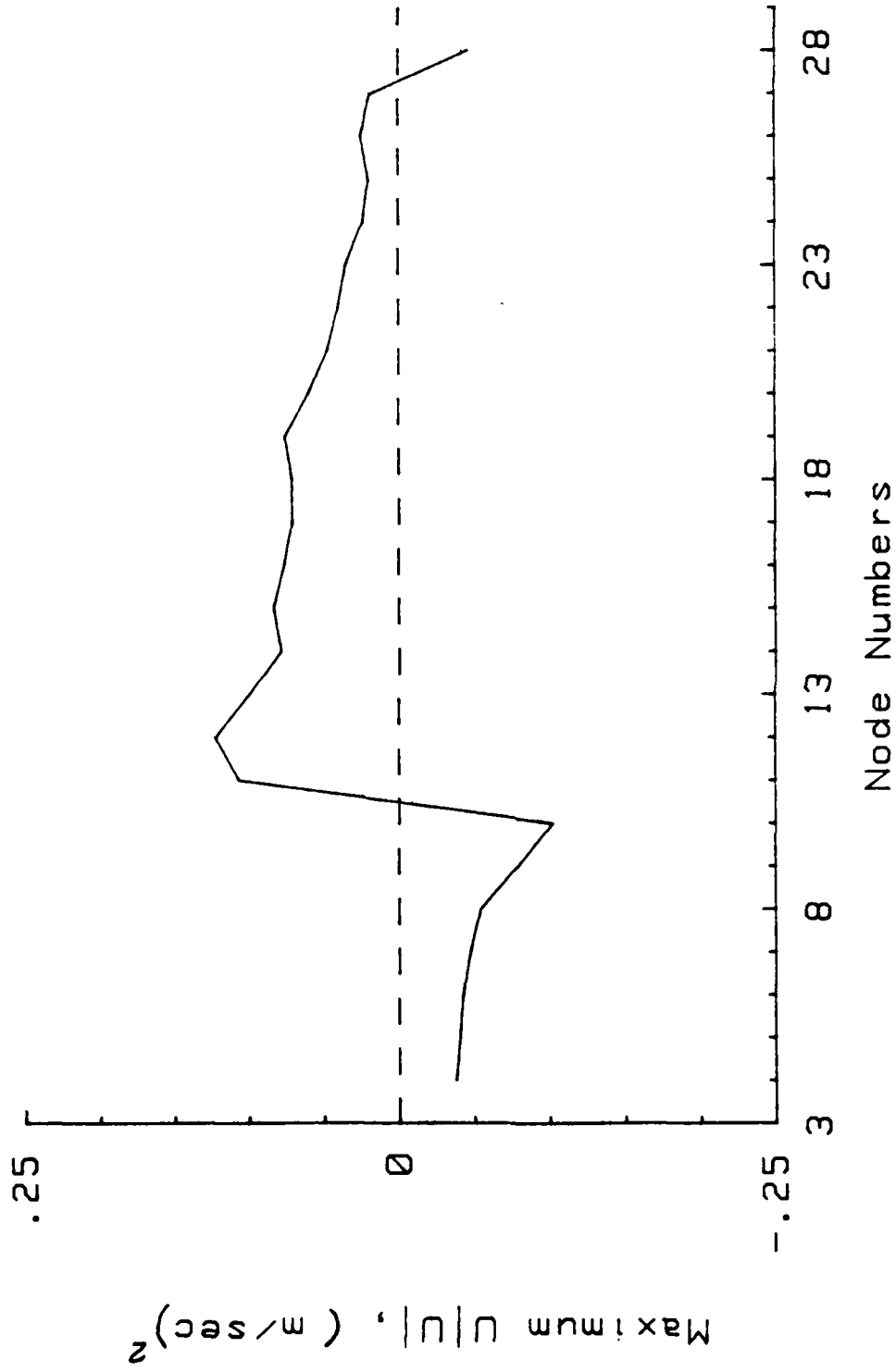


Figure 17. Maximum near-bed velocities squared and directions along the harbor channel for 4,500-cfs plan test

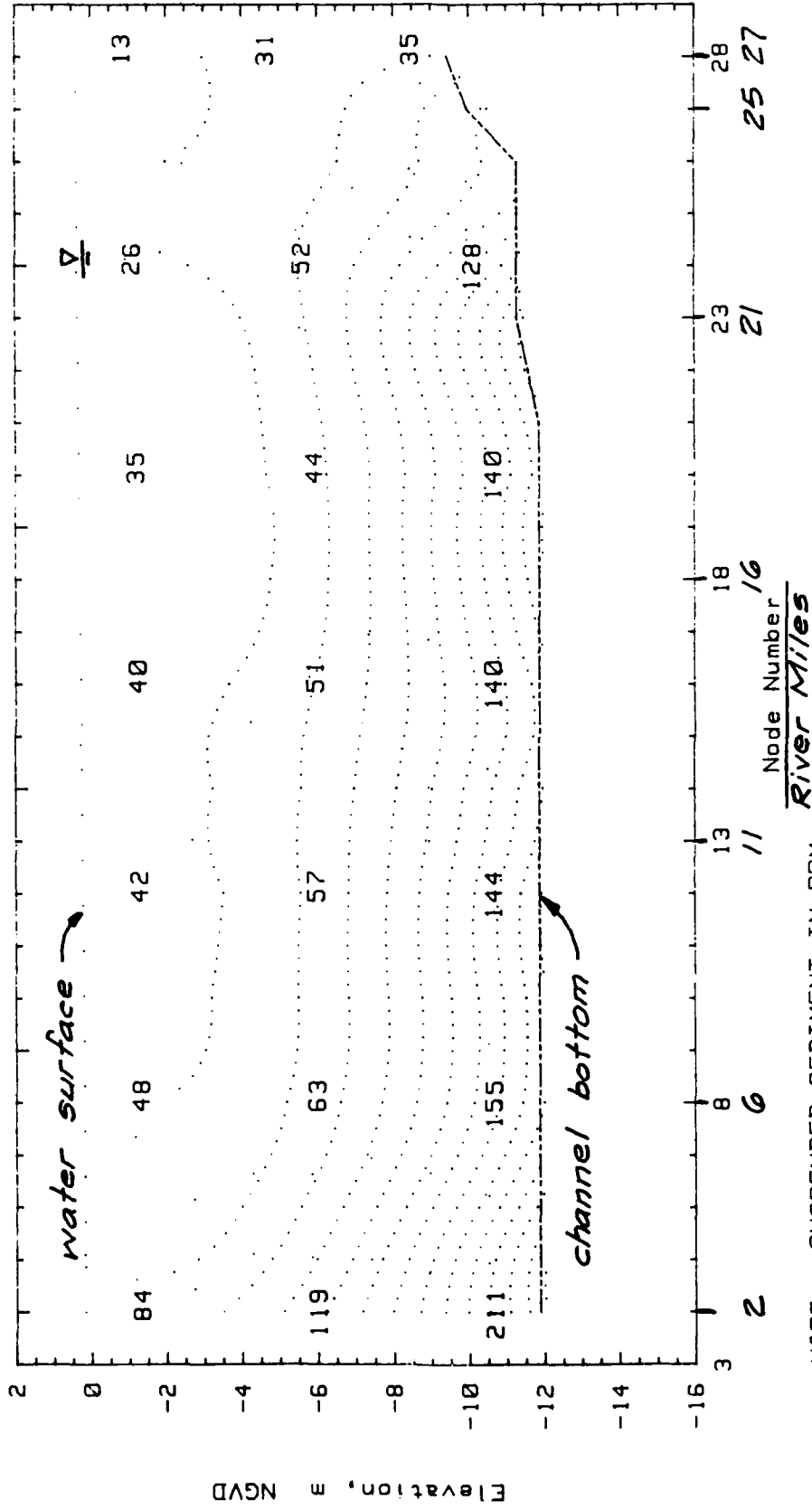
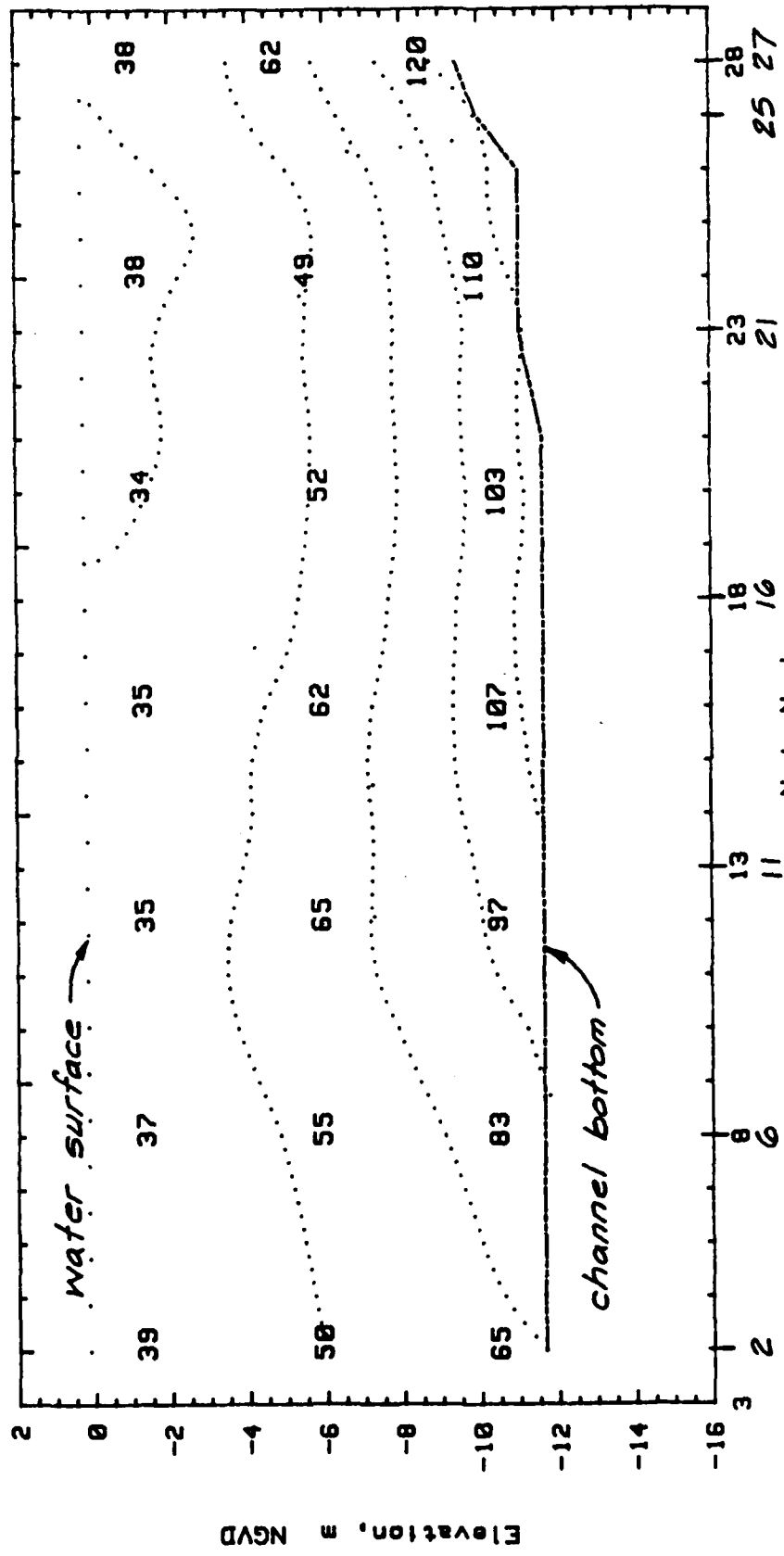


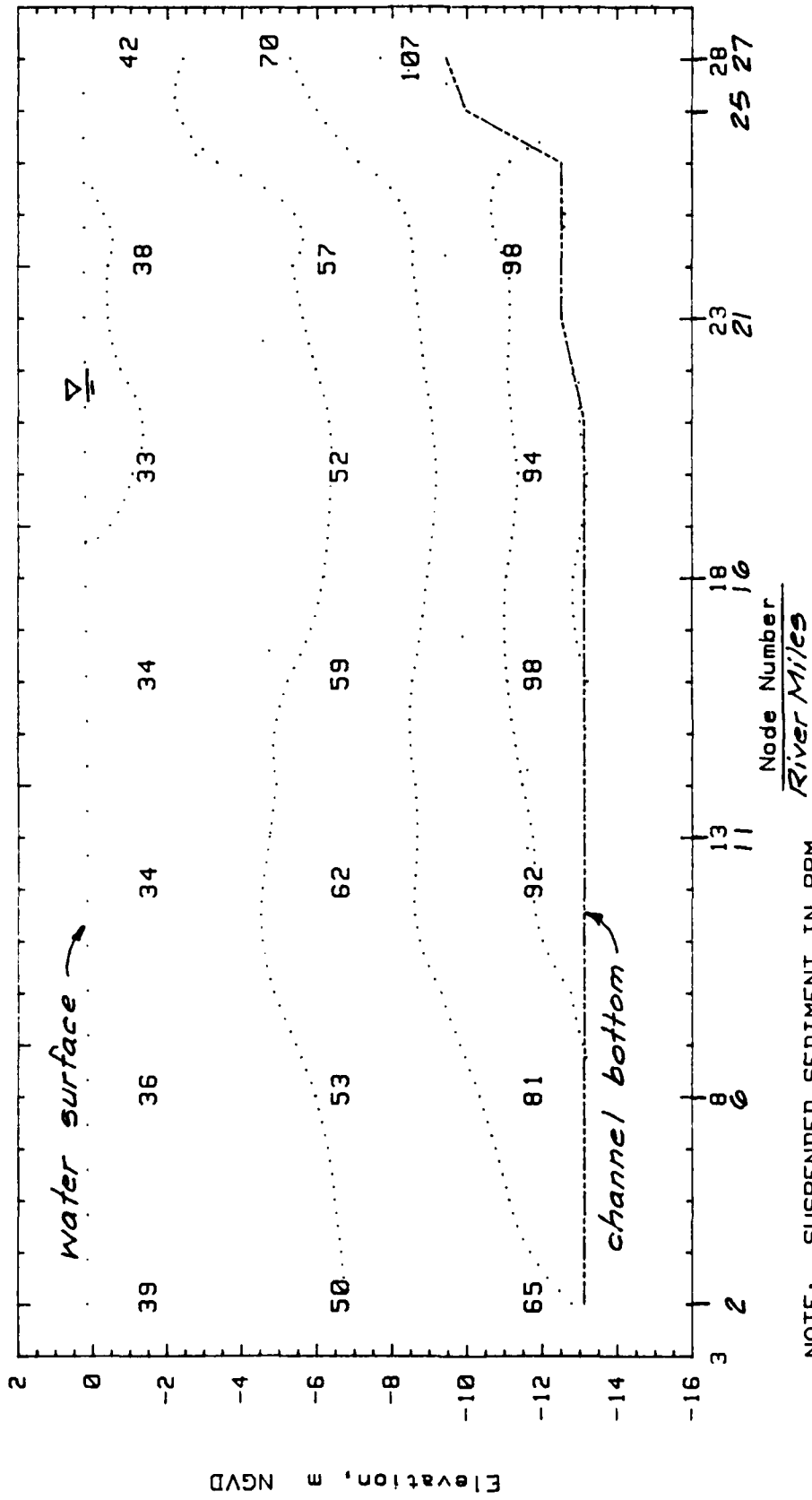
Figure 18. Profile of suspended sediment values along the harbor channel for 15,600-cfs base test



NOTE: SUSPENDED SEDIMENT IN PPM
 CONTOUR INTERVAL 25 PPM

GEOMETRIC DISTORTION-1207:1

Figure 19. Profile of suspended sediment values along the harbor channel for 4,500-cfs base test



GEOMETRIC DISTORTION-1207:1

Figure 20. Profile of suspended values along the harbor channel for 4,500-cfs plan test

APPENDIX A: SHOALING RATES AT 3,000- TO 4,500-CFS INFLOW

Purpose

1. The purpose of this appendix is to present an analysis of the differences in Charleston Harbor shoaling for the range of inflows from 3,000 to 4,500 cfs.

Brief Review of Previous Shoaling Analyses

2. Study of the causes of the Charleston Harbor shoaling began shortly after the diversion of the Santee River's flow into the Cooper River in 1942. A model study at the US Army Engineer Waterways Experiment Station (USAEWES) was authorized in 1947, and complementary studies were carried at the US Army Engineer District (USAED), Charleston, in the late 1940's. By the 1950's, experience with the diversion and investigations into the harbor shoaling had identified the diversion as the major cause of the shoaling problem.

3. Prototype investigations by USAED, Charleston (1954),* showed the suspended material in the Cooper River to be identical to those in the shoal material. Kaolinite was identified as the primary mineral in the fines. Settling tests showed that 75 percent of the particulates settled at less than 0.001 fps. Shoal densities and grain size distributions were measured. By all indications, the shoal material was characteristic of fine-grained, cohesive sediments. During freshet conditions, highly turbid waters were observed to pass from the Lake Moultrie Reservoir into the Cooper River and fill the harbor with a reddish hue. Thin laminations of slick clayey materials, notable by their distinctive color and texture, formed on tidal flats and beaches in several areas.

4. This study concluded that the rivers were the largest initial source, with settling occurring in areas of relative stagnation, trapping material in the flood-dominated bottom levels of the estuary. Material near the bed can move, dependent on its density and viscosity, until it has the opportunity to harden sufficiently.

* References cited in this appendix can be found at the end of the main body of the report.

5. The earliest model study (USAEWES 1957) concluded that more than 99 percent of the shoaling increase was due to the diversion, brought on by the following factors:

- a. A density flow superimposed on the tidal flow that produced strong flood-dominated flows near the bed, preventing the estuary from disgorging its load to the sea.
- b. Increased colloids and dissolved material available to shoal the harbor, both from suspended load in the river and from erosion of the upper channel (assumed to have equal magnitudes).

Channel deepening from -30 to -35 ft mean low water (mlw) was found to have caused only a minor increase in harbor shoaling. Rediversion model tests performed at 2,500- and 5,000-cfs inflow implied that about 3,000 cfs was the maximum tolerable to harbor stratification, but the report cautioned that no single flow was best for the entire harbor.

6. The latest study of shoaling conditions in Charleston Harbor and the effect of rediversion on shoaling was performed by the US Geological Survey (Patterson 1983). An attempt was made to quantify sediment sources for the system, and balance them against amounts of sediment removed by dredging and storage in deposits. Patterson gathered existing information to estimate rates of sediment inflow, removal, and accumulation. Dredging records, hydrographic surveys, maps, charts, hydrologic data, unpublished files, and knowledgeable individuals were sources of information for this study.

7. Patterson divided the data into approximately 20-year periods to identify trends. The sediment sources identified (and mean annual values for 1966 through 1982) included the following:

- a. Pinopolis discharge (0.8 million cubic yards).
- b. Cooper River scour (0.25 million cubic yards).
- c. Background sources including diatom plankton, marsh vegetation, urban storm runoff, wastewater, and shoreline erosion (0.2, 0.6, 0.15, 0.02, and 0.3 million cubic yards, respectively).
- d. Unknown (ocean and unspecified) sources (3.4 million cubic yards).

The unknown source magnitude was estimated by subtracting the known inputs from the total of the amounts removed and accumulated. This study was able to account for only less than half of the shoaling by known sediment sources. The Pinopolis discharge of suspended sediments (which was estimated using a number of different methods) accounted for only about 15 percent of shoaling volumes.

8. By the early 1960's Charleston Harbor's shoaling rate had stabilized with respect to the diversion. Dredging became more effective in the early 1950's, and river channel erosion greatly diminished.

9. Sediment sources were projected for 3,000-cfs inflow to predict the effect of redirection on shoaling rates. A shoaling reduction of 40 to 75 percent was predicted for the Cooper River redirection, based largely on the unknown component.

Shoaling Processes in Charleston Harbor

10. The 1942 diversion resulted in an increase in freshwater inflow from about 600 to 15,600 cfs, and caused about a 36-fold increase in inner harbor dredging (from 120,000 cu yd per year in 1953 exclusive of bar and jetty channel) as well as substantial increases in other areas (USAEWES 1957). Three hydrodynamic sediment traps were created by the diversion, and were largely responsible for increased retention of shoaling material and buildup of unconsolidated mud throughout the estuary:

- a. Vertical density stratification increased drastically and trapped sediments near the bed.
- b. Net tidal-averaged circulation patterns changed and trapped near-bed suspended sediments in developed areas of the estuary.
- c. Once concentrated and deposited, sediments were trapped in unconsolidated mud and isolated to a large extent from transport by turbulent tidal flows.

The increase in project channel depth that occurred at about the same time as the diversion did not have an important effect on harbor shoaling.

11. The major effects of redirection on shoaling for both the 4,500- and 3,000-cfs weekly average flows were as follows:

- a. Reduce vertical density stratification, thus improving vertical mixing, preventing sediments from being trapped near the bed, and improving sediment flushing for the harbor.
- b. Move the null area of vertical circulation upstream, thus reducing suspended sediment accumulation and unconsolidated mud formation in project and facility areas.
- c. Reduce sediment and nutrient loadings to the harbor.

Vertical density stratification, which is created by vertical salinity stratification, damps vertical mixing. The null area of vertical circulation is where near-bed net (tidal-averaged) velocities are neither landward nor

seaward, and thus is an area of converging net bottom flow. Organic materials contribute to shoaling directly, and foster the coagulation of inorganic sediments.

12. The largest reservoir of potential channel shoaling material is now the vast (20- to 30-million-cubic-yard) blanket of unconsolidated mud that covers the floor of the estuary. This material has densities between 1.22 and about 1.05 g/cu cm, and consistencies between that of mayonnaise and pea soup. Unconsolidated mud has been observed to move within estuaries. It can move longitudinally landward or seaward in response to changing tidal and fresh-water inflow conditions, or laterally due to channel slopes or special flow conditions. These sediments are not generally moved with the net estuarine circulation as are suspended sediments. Unconsolidated muds slump or move only with stronger tidal flows near the bed, and tend to accumulate in deeper areas of relative stagnation.

Prediction Method

13. Prediction of the difference in shoaling between 3,000 and 4,500 cfs was made using a method similar to that used by Patterson (1983). A sediment budget was constructed for Charleston Harbor that identified various sediment source components. Data on average annual sediment sources from 1966 through 1982 were used. The effect of redirection on each component was estimated to make shoaling predictions. Overall shoaling for the Charleston Harbor was considered.

14. The latest Charleston District estimate of the 1965 through 1984 average annual gross dredging for Charleston Harbor (6.19 million cubic yards per year) was used in this analysis, and was somewhat lower than Patterson's value of 7.6 million cubic yards per year. The Charleston District value includes the Naval Ammunition Depot (NAD) channel, shoals 1-6, Customs House and tidewater reaches, Shipyard River, anchorage, and entrance channel dredging. Annual dredging rates and locations of these major shoals are given in Table A1. It does not include Navy and other slips, which amounted to 3.13 million cubic yards per year average for the period 1953 through 1963. The pier-slip contribution to 1965 through 1984 dredging is not known, but is probably lower than the older average. The estimated difference in shoaling rates between 3,000 and 4,500 cfs was not affected by this omission. Runback,

the difference between gross dredging volumes and permanent removal, was assumed to be 22 percent.

15. Plant contributions to shoaling by marshes and diatom plankton were treated separately in this analysis, as they are considered to depend on inflow. The high level of productivity in estuarine and coastal waters has been attributed in part to enrichment by nutrients carried by river waters (Parsons and Takahashi 1973). Additional estuarine biological productivity enhancement comes from the mixing of fresh water (in which phosphorus limits plant growth) with ocean water (in which nitrogen usually limits plant growth), and from the entrainment of deeper, nutrient-rich coastal waters by estuarine flows. Plant production contributions were assumed to come from dissolved and particulate nutrients, largely nitrogenous materials, carried by the inflow.

Expected Shoaling

16. The difference in direct sediment inflow and plant production between 4,500- and 3,000-cfs weekly average flows will amount to about 160,000 cu yd of shoaling material annually (Table A2). Sediment inflow and plant production contributions to shoaling are expected to be proportional to Pinopolis inflow.

17. The unknown sediment source referred to in Table A2 could be made up largely from sediments of ocean origin. Reduction of the unknown source was related to the improved sediment flushing efficiency of the harbor, and therefore inversely proportional to the vertical density stratification observed during flow testing surveys. Scour in the Cooper River is expected to be eliminated for both 3,000- and 4,500-cfs flows.

18. The overall shoaling reduction predicted in Table A2 for 3,000 cfs (74 percent) is slightly greater than the Charleston District overall 1966 estimate (71 percent), and slightly less than the upper limit of Patterson's (1983) predicted range (40-75 percent).

19. The overall difference in dredged volumes between 4,500- and 3,000-cfs weekly average flow will most likely be about 200,000 cu yd annually.

Entrance Channel Shoaling

20. The overall shoaling estimates presented in the preceding paragraphs included the entrance channel. Entrance channel shoaling will be considered separately in this section because of dredging cost concerns for this area and because of the paradoxical nature of shoaling seaward from a harbor many experts have declared to be an efficient sediment trap.

21. Early studies described Charleston Harbor entrance channel shoaling material as coarse-grained. Patterson (1983) compiled prediversion dredging volumes for the entrance channel. Long-term averages were less than 267,000 cu yd per year. Recently the Charleston District has identified entrance channel shoaling as fine-grained. Average entrance channel dredging was 1.24 million cubic yards per year for 1965 through 1984.

22. Rough calculations of deposition rates from sediment suspensions were made for the entrance channel using reasonable values for settling velocity (0.01 cm/sec), near-bed suspension concentration (200 mg/l), and the frequency of deposition time. The frequency of deposition time was estimated using an assumed critical shear stress for deposition (0.05 Pa) and compiled coastal currents for the area (0.3 to 0.8 knots) as 8 percent (about 30 days per year). To balance the observed shoaling mass (specific weight of shoal material times shoal volume divided by shoal area) with calculated deposition from suspension required unreasonable values for depositional frequency (267 days per year) or for near-bed concentration (1,780 mg/l). Therefore, it is difficult to account for shoaling in the entrance channel by settling from suspension, even when the possibility of reerosion of deposited sediments by storm action is totally ignored. Therefore, even when the possibility of reerosion of deposited sediments by storm action was ignored, only a small part of the shoaling in the entrance channel was attributed to settling from suspension.

23. Entrance channel shoaling increases have probably been caused by near-bed movements of unconsolidated mud. Ebbing tidal flows transported sediments out of the estuary, and they became stranded in the outer entrance channel where tidal flood flows were insufficient to return them.

24. It is reasonable to assume that there will be a considerable reduction in entrance channel shoaling after rediversion and a stabilization period. This was also the opinion of the Committee on Tidal Hydraulics

(1966). The shoaling reduction in this area will be of the same order of magnitude as the predicted overall reduction. The unconsolidated mud shoaling source will diminish over the next decade--some of it dredged from channel sites, some flushed seaward from the harbor, and some hardening in place. Suspended sediment flushed seaward is not expected to deposit rapidly enough to increase entrance channel shoaling.

Table A1
Annual Dredging Rates and
Locations of Major Inner Harbor Shoals, 1965-1984*

<u>Shoal/Reach</u>	<u>Annual Gross Yardage 1,000 cu yd</u>	<u>River Mile</u>
Anchorage	767	6.5- 7.7
Tidewater	563	9.1- 9.7
6A	547	9.7-11.1
6B	37	11.4-12.2
6C	263	9.9-10.7
6	115	11.6-12.3
Shipyard River	780	13.0-13.7
5A	406	13.2-14.1
4	170	16.2-17.0
3	37	17.7-18.9
1 and 2	300	18.9-20.4
NAD	828	20.9-23.1
Total	<u>4,813</u>	

* Data supplied by B. Kyzer, USAED, Charleston.

Table A2
Effects of Pinopolis Inflow on Sediment Sources and Shoaling
Volumes for Charleston Harbor

Pinopolis Inflow Weekly Average cfs	Shoaling Volumes,* million cubic yards				Total	Shoaling Reduction percent
	Cooper Scour ††	Sediment Inflow ††	Plant Production** ††	Background ††		
15,600	0.25††	0.80††	0.80††	0.45††	4.8	0
3,000	0.0	0.16	0.16	0.45	1.3	74
4,500	0.0	0.24	0.24	0.45	1.4	70

* Dredged volumes are expected to be 1.28 times shoaling volumes to account for runback.

** Includes diatom plankton and marsh vegetation. See paragraph 15 in this appendix.

† Urban runoff and shoreline erosion from Patterson (1983).

†† Ocean and other sediment sources. Assumed to be related to estuarine trap efficiency. See paragraph 17 in this appendix.

† (1 - total shoaling volume/4.8) × 100.

†† Data from Patterson (1983).

APPENDIX B: FLOW AND SALINITY MODEL

1. This appendix presents and describes the mathematical equations that make up the flow and salinity portions of the FIBS model used in this study. Due to the complicated nature of this subject, the description will be limited to an overview. Blumberg (1977)* and Wang (1983 and 1984) describe similar laterally averaged flow and salinity models. Appendix C describes the sediment transport model equations, Appendix D describes the fluid mud modeling, and Appendices E and F contain definitions and notation used throughout the report for reference.

Equations

2. The following governing laterally averaged dynamic differential equations describe estuarine flow, mixing, and circulation:

- a. The vertically integrated continuity equation.
- b. The horizontal momentum equation.
- c. The continuity equation.
- d. The salinity transport equation.

Additional terms were included in the equations to describe both lateral inflows and tributaries. The following algebraic expressions are required to dynamically modify, or close, the set of differential equations:

- a. The equation of state.
- b. The friction coefficient equation.
- c. The equations for vertical eddy diffusivities for mass and momentum.

An improved vertical eddy diffusivity closure was made using a differential equation for the transport of turbulent kinetic energy.

3. Laterally averaged equations use values averaged across sections at certain increments of depth. The channel widths are specified at each node depth as indicated in the hypothetical channel cross section (Figure B1).

* References cited in this appendix can be found at the end of the main body of the report.

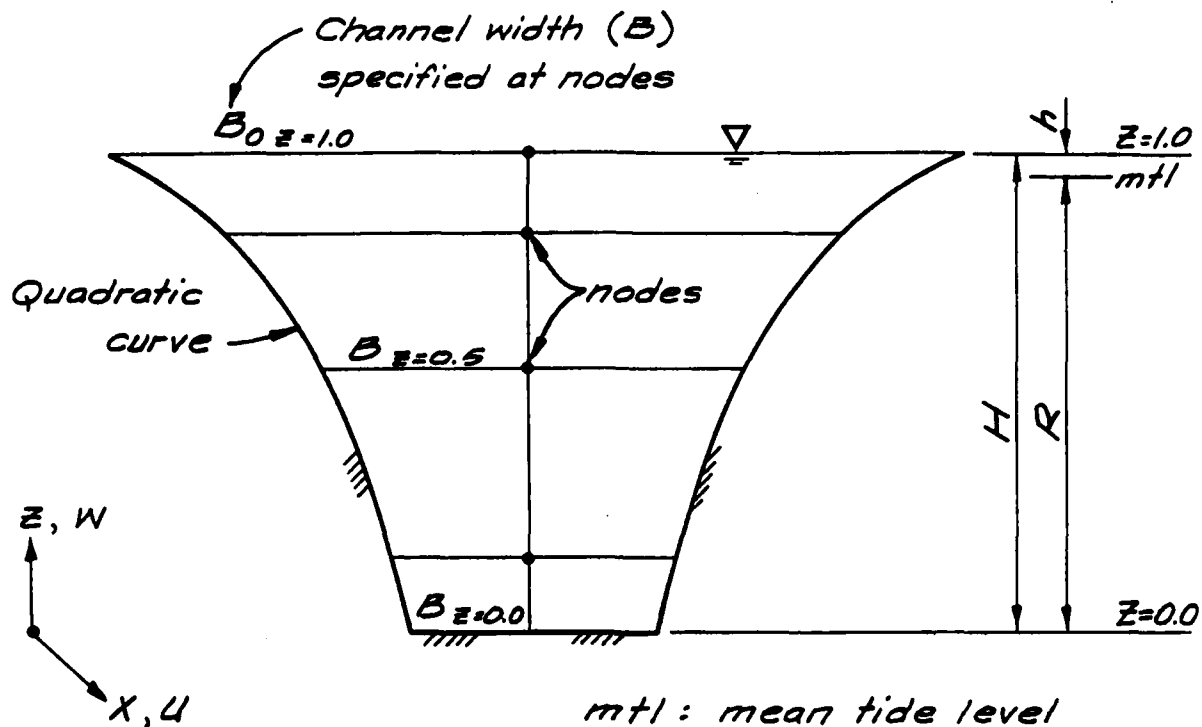


Figure B1. Hypothetical channel cross section (looking seaward)

Vertically integrated continuity equation:

$$\frac{\partial (B_o h)}{\partial t} + \frac{\partial}{\partial X} \int_{-R}^h (UB) dz - \frac{q}{B_o \Delta_e} = 0 \quad (B1)$$

Horizontal momentum equation:

$$\begin{aligned} \frac{\partial}{\partial t} (UB) + \frac{\partial}{\partial X} (UUB) - BN_x \frac{\partial^2 U}{\partial X^2} + \frac{\partial}{\partial Z} (UWB - BN_z \frac{\partial U}{\partial Z}) \\ + Cd U|U| \left| \frac{\partial B}{\partial Z} \right| + gB \frac{\partial h}{\partial X} + g \frac{B}{\rho_o} \int_z^h \left(\frac{\partial \rho}{\partial X} dz \right) = 0 \end{aligned} \quad (B2)$$

Continuity equation in a vertical plane:

$$\frac{\partial (UB)}{\partial X} + \frac{\partial}{\partial X} (WB) = 0 \quad (B3)$$

Salinity transport equation:

$$\frac{\partial(SB)}{\partial t} + \frac{\partial}{\partial X} (SUB) - BK_x \frac{\partial^2 S}{\partial X^2} + \frac{\partial}{\partial Z} (SWB - BK_z \frac{\partial S}{\partial Z}) - \frac{S_l q}{H \Delta_e \int_{-R}^h B dZ} = 0 \quad (B4)$$

Equation of state:

$$\rho = \rho_o (1 + C1 \cdot S) \quad (B5)$$

where

ρ_o = freshwater reference density (0.9987 g/cu cm)

C1 = constant (1.3751 E-6)

S = salinity parameter expressed here as chlorinity, ppm

Bed friction:

$$Cd(x) = \frac{gn^2}{2.22 R^{1/3}} \quad (B6)$$

where n is Manning's coefficient of friction.

Vertical eddy diffusivities:

4. Under homogeneous conditions, characteristic eddy diffusivities are $N_{zo} = K_{zo} = K'_z$, where K'_z is a specified constant. The effects of vertical density stratification are included using the method of Munk and Anderson (1948).* Thus:

$$K_z = K_{zo} (1 + 3.33 Ri)^{-(3/2)},$$

and

$$N_z = N_{zo} (1 + 10 Ri)^{-(1/2)},$$

* References cited in this appendix can be found at the end of the main body of the report.

where

$$Ri = \frac{-g}{\rho_o} \frac{\partial \rho / \partial Z}{(\partial U / \partial Z)^2},$$

Then at depth,

$$K_z(z) = F_z(z) \cdot K'_z, \quad (B7)$$

where F_z is a similarity distribution for vertical eddy diffusivity.

Turbulent kinetic energy:

5. Instead of assigning a value to K'_z , the model will optionally use turbulent kinetic energy κ generated, dissipated, and transported by the flow to calculate vertical diffusivities. The scheme employed is similar to that described by Smith and Takhar (1979) and Smith (1982). Transport is computed in one dimension by:

$$\frac{\partial \kappa}{\partial t} + \bar{U} \frac{\partial \kappa}{\partial X} - D_x \frac{\partial^2 \kappa}{\partial X^2} - \frac{\kappa \ell^q}{H \Delta_e \int_{-R}^h B dz} - P_k + \epsilon = 0 \quad (B8)$$

where P_k is production of turbulent kinetic energy, and

$$P_k = 22.4 \left(\frac{U_*^2}{R} \right)$$

ϵ is dissipation, and

$$\epsilon = 1.66 \left(\frac{\kappa^{3/2}}{R} \right)$$

and \bar{U} is the cross-sectional average velocity,

$$\bar{U} = \frac{1}{H} \int_{-R}^h U dz$$

Then, $K_{z0} = N_{z0} = 0.09 \kappa^{1/2} R$, and the values for K_z , N_z , $K_z(z)$ and $N_z(z)$ are computed as previously described.

Boundary Conditions

Ocean boundary

6. In general, the varying tidal conditions are controlled at the ocean boundary of the model mesh. This is accomplished by specifying a tidal water level target value at each time-step in the form of $h'(t) \Big|_{X=0} = f(t)$. The model has the capability to synthesize tidal sequences for any specified starting time using 12 constituents and harmonic coefficients provided by the National Ocean Survey. The individual constituents used included M2, S2, K1, O1, P1, N2, L2, Sa, M_sf, Mf, Mm, and Ssa.

7. A nonreflecting ocean boundary was computed for this study by replacing the vertically integrated continuity equation with the following expression:

$$\frac{\partial h}{\partial t} + C_w \frac{\partial h}{\partial X} = - \left(\frac{h(t) - h'(t)}{T_f} \right) \quad (B9)$$

where

$$C_w = (gH)^{1/2} \Big|_{X=0}$$

and T_f is a damping parameter (found to be about 500 sec). This method is similar to that presented by Blumberg and Kantha (1985), and allows long waves, or water level perturbations, originating within the model domain to pass through the ocean boundary without reflection. The non-reflecting ocean boundary permits faster stability within the model, and in this study, the model reached the stable condition in two tidal cycles. During the flood tidal phases, salinity concentration was specified at the ocean boundary; otherwise the transport boundary was unconstrained.

Upstream boundary

8. Velocities are specified at upstream inflow boundaries and flow rates are specified at lateral inflows. In this study, the condition $U(t) = 0$ was specified at Pinopolis, the upstream end of the model, and a lateral inflow was specified at the adjacent element to represent the hydro-power flow release. The Cooper River contributes almost all of the freshwater inflow to the system and is controlled at the Pinopolis Dam. Salinity

concentrations (usually zero) were specified at these inflows.

Bottom boundary

9. For this study, the bottom boundary ($Z = 0.0$) was considered to be a slip-flow boundary. The shear stress was imposed by the equation:

$$N_z \frac{\partial U}{\partial Z} = Cd U|U| \quad (B10)$$

Optionally, the model will extrapolate shear stress linearly from within the flow to the bottom boundary using a method suggested by Smith (1982). Within the salinity transport equation, no flux is allowed at the bottom boundary and:

$$US + K_z \frac{\partial S}{\partial Z} = 0 \quad (B11)$$

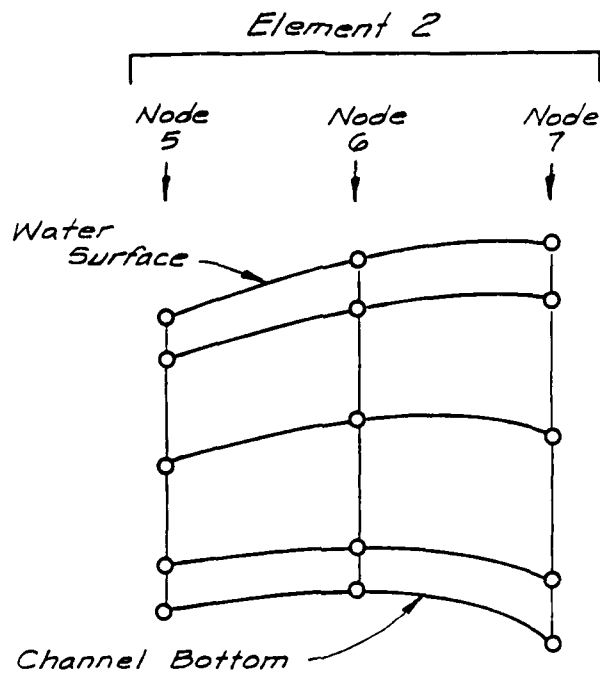
Vertically Stretching Coordinates

10. In the vertical or Z-direction, computational nodes are assigned to the surface, intermediate, and bottom levels. When changes occur in the water levels, all nodes except the bottom node move, or stretch, to conform with the depth of flow. The typical configuration of the nodes within an element are shown in Figure B2. The stretching coordinates system introduces new terms into the governing differential equations. A derivative in some level of the X-direction is calculated by the following expression:

$$\frac{\partial}{\partial X} = \frac{\partial}{\Delta_e \partial x} - \left(\frac{Z}{R\Delta_e} \frac{\partial h}{\partial x} \frac{\partial}{\partial Z} + \frac{(1-z)}{R\Delta_e} \frac{\partial R}{\partial x} \right) \frac{\partial}{\partial Z} \quad (B12)$$

The X and Z are the actual world coordinates. The x and z are the nondimensional element coordinates that vary in each element from 0.0 to 1.0 upstream and vertically upward, respectively. The two coordinate systems are related by

$$\frac{\partial}{\partial Z} = \frac{1}{H} \frac{\partial}{dz} \quad (B13)$$



Note: slopes are quadratic (exaggerated here).

Figure B2. Example computational element from schematic mesh showing stretching coordinates and nodes

$$\frac{\partial}{\partial X} \approx \frac{1}{\Delta_e} \frac{\partial}{\partial x} \quad (\text{B14})$$

where Δ_e is the element length. This method is similar to the finite-difference methods presented by Sheng (1983).

Solutions of the Equations

11. The governing equations were solved over the previously described finite elements, using an explicit orthogonal collocation method of weighted residuals. Weighted residual methods can be used to expand an unknown solution in a set of trial functions T over a domain v . The collocation method applies weighting functions (w_j , a Dirac delta function) to the trial functions, chosen to be set of orthogonal polynomials. The node locations x_j satisfy the roots of the polynomials. The form of the collocation method is now

$$\int_v w_j^T dv = T \Big|_{x_j} \quad (\text{B15})$$

where $w_j = \delta(x - x_j)$.

12. Instead of solving for the unknown trial function coefficients, a major simplification described by Finlayson (1972) is that the solution can be derived in terms of values at the collocation nodes. The nodes are located at Gauss points for this purpose, and the method is known as orthogonal collocation. The derivatives and integrals can therefore be expressed in terms of values of the function at the collocation nodes by

$$\frac{dr}{dx} \equiv A r \text{ and } \frac{d^2r}{dx^2} \equiv B r \quad (\text{B16})$$

The matrices A and B are computed from the trial functions.

Integration in Time

13. An explicit time integration method was used to compute variables dynamically over time. The fourth-order Runge-Kutta method was used in this study. This method is very accurate, and often used to solve "stiff" equation sets, equations with distinct stability limits. Results were found to be independent of time-step Δt up to a Courant number $\Delta_e / \Delta t \cdot Cw$ of 1.0 (or 2.0 based on longitudinal node spacing). With the initial conditions (t_n, y_n) over Δt , the function $y'(t) = f(t, y)$ is solved in four steps:

$$\underline{a.} \quad K_0 = \Delta t \cdot f(t_n, y_n) ,$$

$$\underline{b.} \quad K_1 = \Delta t \cdot f\left(t_n + \frac{\Delta t}{2}, y_n + \frac{K_0}{2}\right) ,$$

$$\underline{c.} \quad K_2 = \Delta t \cdot f\left(t_n + \frac{\Delta t}{2}, y_n + \frac{K_1}{2}\right) ,$$

$$\underline{d.} \quad K_3 = \Delta t \cdot f\left(t_n + \Delta t, y_n + K_2\right) ,$$

Finally, the result of the four steps are combined to complete the time-step:

$$y_{n+1} = y_n + \frac{1}{6} (K_0 + 2K_1 + 2K_2 + K_3) \quad (\text{B17})$$

APPENDIX C: SEDIMENT TRANSPORT MODEL EQUATIONS

1. This appendix presents and describes the mathematical equations that make up the sediment transport algorithms for fine-grain sediment within the FIBS model. The governing differential transport equation is presented first, with the remainder of this appendix briefly describing the various aspects of sediment transport and the corresponding mathematical treatments.

Characterization of Suspended Sediment

2. Sediment in suspension represent some specific fraction of the bed material in a harbor or estuary. Sediment is physically sorted or fractionated during suspended transport. Fine-grained sediments are hydraulically transported almost entirely in suspension rather than as bed load. Because of the differences in cohesion, settling characteristics, etc., for silts (4-72 μm) and clays (0.45-4 μm), fine-grained sediments are sometimes characterized as a sum of several fractions or components. The fine-grained material can also contain an organic fraction, which behaves similar to cohesive sediments.

3. Fine-grained sediments exhibit some degree of cohesion; thus clay and organic solid particles aggregate under normal estuarine conditions. The state or degree of aggregation affects the deposition, erosion, and settling processes, described later, and depends on sediment concentration, salinity, turbulence in the flow, pH, temperature, and other physical factors.

Governing Transport Equation

4. The governing differential equation for laterally averaged fine-grained sediment transport is

$$\frac{\partial(CB)}{\partial t} + \frac{\partial(CUB)}{\partial X} - BK_x \frac{\partial^2 C}{\partial X^2} + \frac{\partial}{\partial Z} \left(CW_B - CW_s B - BK_z \frac{\partial C}{\partial Z} \right) - \frac{C_{\ell} q}{h} + D - E = 0 \quad (C1)$$

$$HA_e \int_{-R}^0 B dz$$

where

C = concentration of suspended sediment

W_s = settling velocity

D = deposition

E = erosion.

Each of these terms is described by a set of algebraic expressions, and is discussed in the following sections.

Settling

5. Settling is that component of suspended particle or aggregate motion caused by the balance between gravity and viscous drag forces. Settling rates are therefore defined in quiescent native fluid. Settling characteristics affect the rates of deposition and the vertical distribution of suspended material within the water column.

6. Aggregation is very important to cohesive sediment settling rates, and is responsible for clay deposition in estuaries and marine environments. Aggregation of a particular sediment particle suspension depends primarily on suspended sediment concentration, current shear or velocity gradients, and salinity. Previous experiments on the effects of current shear on settling found impacts at shear rates above those encountered within most natural flows (Hunt 1982).* Salinity effects on aggregation are greatest between 0- and 4-ppt concentration. Most coastal and estuarine harbors are almost always above this range.

7. Three ranges of concentration-dependent settling usually occur. At low concentrations, aggregate and particle interaction is minimal, and settling is independent of concentration. At intermediate concentration, settling is enhanced by concentration because of increased aggregation and particle interaction. At high concentrations, aggregate and particle interaction hinders settling.

8. Suspended sediment concentrations are usually in the enhanced-settling range. The dependence of settling velocity W_s in the

* References cited in this appendix can be found at the end of the main body of the report.

enhanced-settling concentration range has the functional form (Ariathurai, MacArthur, and Krone 1977):

$$W_s = A_1 C^{A_2} \quad (C2)$$

where A_1 is a constant and A_2 is the enhanced settling exponent. The exponent A_2 is usually found to be close to 1.33. The concentration range over which Equation C1 applies varies with the cohesive properties of the sediment. Generally the lower bound is in the range of 10-200 mg/l, and the upper bound is in the range of 2,000-75,000 mg/l.

9. Fine-grained sediment suspensions usually have a range or distribution of W_s . Clay and fine silt fractions aggregate to form a relatively uniform settling aggregate. Medium and coarse silt fractions settle at higher rates, and are less dependent on concentration than the clay fraction. Settling tests can be used to determine the magnitude and distribution of W_s at various suspended sediment concentrations for the finer fractions of the material. Such testing is done in the field or laboratory, or a combination of both.

Deposition

10. Deposition D , or flux of sediment material to the bed, is the sum over a number of fractions of settling flux times deposition probability (Mehta et al. 1986)

$$D = \sum_{j=1}^k P_j W_{s_j} C_j \quad (C3)$$

where

k = number of sediment fractions

P = probability that an aggregate which has reached the bed will remain there

C = concentration just above the bed

j = subscript indicating a sediment fraction

P varies linearly from 0 at a bed shear stress equal to the critical shear

for deposition, $\tau_b = \tau_{cd}$, to 1 at zero bed shear stress, $\tau_b = 0$. The functional form $1 - (\tau_b/\tau_{cd})$ where $\tau_b < \tau_{cd}$ is used for P (Krone 1962). Laboratory deposition testing can be used to determine τ_{cd} and the magnitude of the product PW_g for each sediment fraction identified.

11. A suspension of uniform material in a steady, uniform flow will either deposit completely or remain entirely suspended depending on whether τ_b is below or above τ_{cd} , according to Equation C3. The consequence of the presence of multiple sediment fractions in a suspension is that, under a given flow condition, some sediment fractions may deposit while others may remain in suspension. The suspension may therefore transport an equilibrium concentration (some fraction of the source concentration) indefinitely.

12. The values of W_g inferred from deposition tests are smaller than those obtained from quiescent settling tube tests. The cause for this is not known. However, shear in the flow is greatest just above the bed, and could cause disaggregation and/or produce lift forces counteracting settling at this point.

Resuspension

13. Resuspension of bed material occurs in four modes:

- a. Redispersion
- b. Particle erosion
- c. Significant erosion
- d. Mass erosion

Resuspension is the most difficult fine-grained sedimentation process to either test or form predictions for occurrence. Redispersion occurs when the bed is fluid and particles are fluid supported, lacking interparticle or interaggregate structure. Redispersion proceeds as an entrainment process, scaled to density difference between the fluid mud and overlying water, an appropriate velocity or shear velocity, layer thickness, and viscous effects. Redispersion is initiated at low bed shear stresses and is generally rapid. Mass erosion, on the other hand, has been postulated to occur at very high τ_b , and is initiated when a subbottom layer fails under extreme hydraulic shear conditions, allowing a large bed layer to be carried away by the flow. Mass erosion, under these conditions, is not well documented, and not expected to occur under normal or even severe estuarine conditions. Mass erosion can

also occur in quasi-uniform fluid mud layers on a slope, where stresses increase vertically downward and exceed the shear strength of the layer, and the layer slides as a mass.

14. Particle and significant erosion modes are similar. At τ_b above a critical value, particles or clusters of particles are individually dislodged from the sediment bed as interaggregate bonds are broken. Particle resuspension is related to the shear stress in excess of a critical value, and to an erosion rate constant M (Ariathurai, MacArthur, and Krone 1977):

$$E = M \left(\frac{\tau_b}{\tau_c} - 1 \right), \quad \tau_b > \tau_c \quad (C4)$$

where

E = erosion rate

τ_c = critical erosion shear stress for particle erosion

Observed erosion does not follow Equation C4 indefinitely. Suspension concentrations above experimental eroding beds often reach constant or equilibrium values which depend on a combination of the bed shear stress and character of the bed. Equilibrium fine-grained suspensions form as erosion rates decrease with time to zero, while the flow remains constant. Equilibrium fine-grained suspensions have been found to be related not to the transport capacity of the flow (as for sand), but to vertical differences or nonhomogeneity in the bed (either particle characteristics or bed density) or to armoring by selective erosion at the bed surface. Resuspension tests can be used to determine the magnitude of M and τ_c for representative sediment fraction, and to detect the formation and nature of equilibrium suspensions.

15. Typical laboratory relationships between E and τ_b show two regimes or modes of erosion (Hunt 1981). At low shear stresses, erosion has been found to proceed first as surface particle flaking which has a low threshold and a lower value of M . At higher values of τ_b , a break point is passed at which E and M increases sharply. This is termed significant erosion, and was first observed by Partheniades (1962). Visual observations by the author have suggested that significant erosion proceeds as small bed sediment chunks are detached by the smallest scale turbulence (with characteristic lengths on the order of a millimetre). At these higher levels of τ_b ,

the smallest eddies have diminished size and increased energy. During turbulent bursting of the laminar sublayer, small eddies impinge on the bed and dislodge chunks of about their own size. Extrapolating the higher erosion mode yields a relatively high apparent critical erosion threshold. Figure C1 shows an example plot of the general form described.

16. Significant erosion is described similarly:

$$E = M_h \left(\frac{\tau_b}{\tau_{ch}} - 1 \right), \quad \tau_b > \tau_{ch} > \tau_c \quad (C5)$$

where

M_h = the significant erosion rate constant

τ_{ch} = the critical shear stress for significant erosion
 (τ_{ch} is larger than τ_c , and M_h is larger than M)

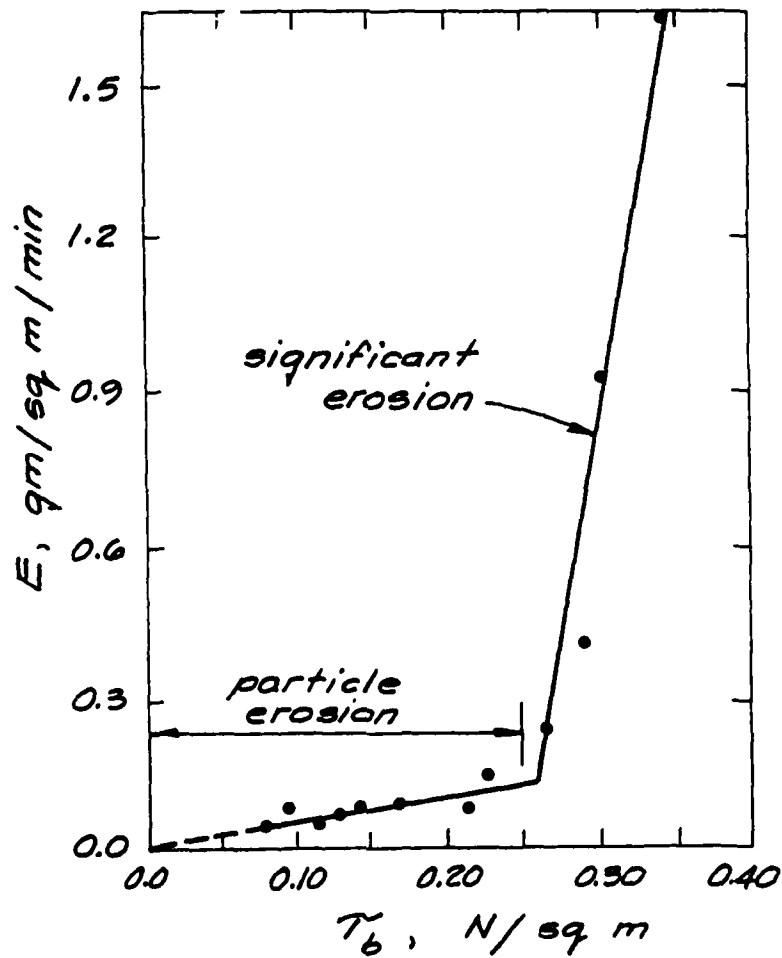


Figure C1. Typical nonlinear erosion behavior of cohesive sediment (data from Hunt 1981)

APPENDIX D: FLUID MUD MODELING

Background

1. The Fine-grained Bed Sediment or FIBS model was formulated to address estuarine conditions where beds are soft muds. Fine-sediment bed conditions are not uniquely related to grain size, but are time-dependent, and related to admixture composition and characteristics. Therefore, bed conditions depend on conditions within the model domain, and are properly an internal rather than external model quantity. The sections that follow describe a dynamic fluid mud model.

2. Fluid mud has concentrations above that at which the maximum settling flux occurs, and below that at which important sedimentary structure forms. Settling flux is the product of settling velocity W_h and concentration. Settling velocities decrease with increased concentration, and a concentration is reached where settling flux (the product of concentration and hindered settling velocity W_h) begins to decrease. This point is the maximum settling flux, and occurs generally at concentrations between 5 and 100 g/l for estuarine cohesive sediments. The behavior of suspensions changes rather abruptly at this concentration, and suspensions begin to settle as a mass. A clear layer forms above a distinct interface. The descent of that interface is associated with consolidation, which is used here to denote volume change by the effect of settling.

3. The settling characteristics of dense suspensions can be determined by column tests conducted over a range of concentrations. Results are fit to any number of functional relationships and used in further numerical analysis. In fluid mud, settling of sediment particles is hindered by particle interaction and by interaction between particles and the pore water. The higher the fluid mud concentration, the more slowly the mixture consolidates by settling. Settling velocities decrease, sometimes sharply, with increasing initial suspension concentration.

4. Several functions can be used to fit high-concentration settling data. The best known functional descriptor of the effect of concentration on hindered-settling velocity appears to be the Richardson-Zaki (1954)* equation:

* References cited in this appendix can be found at the end of the main body of the report.

$$W_h = W_l (1 - B_2 C_s)^{B_1} \quad (D1)$$

where W_h is the hindered-settling velocity, W_l is a reference settling velocity, B_2 is the inverse of the fully-settled concentration, and C_s is the dense suspension concentration. Richardson and Zaki found the exponent B_1 to have a value of 4.7. Sediments from several United States estuaries have been found by the author to fit the Richardson-Zaki equation reasonably well. However, not all data do so (Owen 1970).

Yield stress

5. Rheological tests suggest that fluid mud is a viscoelastic material with the ability to sustain a finite shear stress with zero continuous strain. The yield stress for a number of estuarine muds was determined by Krone (1963), who assumed a Bingham model and found yield stress to be strongly dependent on concentration. Rheological measurements on 20- to 60-g/l suspensions with a rotating cylinder viscometer were found to obey a power law with a slope of 2.5. The yield stress of a sediment material is directly related to the critical shear stress for erosion τ_c , so that

$$\tau_c = D_1 C_s^{D_2} \quad (D2)$$

where C_s is the concentration of fluid mud as dry weight of sediment per unit volume of mud, and D_1 and D_2 are empirical constants. Thus, the hydraulic shear strengths of dense suspensions with 24 g/l and 60 g/l solids varied by about a factor of 10.

6. Likewise, the significant erosion yield or critical stress may be strongly dependent on bed concentration.

$$\tau_{ch} = D_{h1} C_s^{D_{h2}} \quad (D3)$$

where D_{h1} and D_{h2} are empirical constants for significant erosion.

7. The erodibility of estuarine sediments has also been observed to depend on concentration as indicated by Equation D3. Teeter (1987) found the exponent D_{h2} to be 3.38 for San Francisco Bay sediments. The experimental concentration range for the bed was from 275 to 525 g/l.

Model Description

8. A transport theory for the consolidation by hindered settling can be constructed using a form of the vertical transport equation with diffusion and by nondimensionalizing depth as $z = Z/H_s$:

$$\frac{\partial C_s}{\partial t} - \frac{1}{H_s} \frac{\partial}{\partial z} \left(W_h C_s + \frac{K_s}{H_s} \frac{\partial C_s}{\partial z} \right) = 0 \quad (D4)$$

where H_s is the total depth or height of the dense suspension, and K_s is a diffusivity for mass. Diffusive transport in fluid muds could come from bio-turbation (on the order of $1E-7$ sq cm/sec, for example), or from convective instabilities observed in actively settling suspensions. Numerically, the diffusion term was employed to counteract instabilities induced by the boundary conditions required for high deposition rates.

9. Kynch (1952) advanced a kinematic theory for the analysis of hindered-settling tests based on a continuity equation similar to Equation D4. He assumed that settling velocity was a local characteristic dependent on the concentration of the suspension. In the development of his theory, Kynch pointed out that the total derivative of concentration (he used density) for a moving reference point in a dense suspension is equal to the partial derivative of concentration with respect to time plus the convection of the concentration gradient. Thus in the present notation:

$$\frac{dC_s}{dt} = \frac{\partial C_s}{\partial t} + \frac{z}{H_s} \frac{\partial H_s}{\partial t} \frac{\partial C_s}{\partial z} \quad (D5)$$

10. Discontinuities or step changes in the concentration field complicate the analysis of dense suspensions. The interface observed during consolidation experiments is such a discontinuity. Kynch (1952) explained how several transport conditions can produce discontinuities. Discontinuities are associated with the concentration at which the vertical flux is maximum, and other points where the rate of change in vertical flux with respect to concentration is zero. The former condition always occurs, while the latter can occur if the relationship between concentration and settling velocity is not smooth.

11. Solution of the model governing equations requires that the differential equations be replaced by matching conditions at concentration discontinuities. The location of discontinuities therefore becomes part of the problem and must be solved by the model. Numerical solution of transport equations apparently cannot span concentration discontinuities without immediately becoming unstable. Numerical methods used to solve hindered settling discontinuity equations were very similar to those used for flow and salinity.

12. The model mesh was contracted during computations as the dense suspension collapsed so that $z = 1.0$ was fixed to the upper boundary. The height of the suspension to the interface or discontinuity was calculated, for instance, at any time by conservation of mass as

$$\frac{dH_s}{dt} = -W_{h_i} \quad (D6)$$

where the subscript i indicated the location of the interface. A no-flux bottom boundary condition $W_h C = 0$ was imposed at $z = 0$. No condition was required at the upper boundary of the dense suspension since the equation was applied only from fixed bed to the moving interface ($z = 1.0$). Initial height and concentration of the dense suspension were starting points for model computations.

Depositional formation of dense suspensions

13. The concentration of newly deposited material affects the thickness and hydraulic shear strength of the deposit. The concentrations of material as they undergo deposition from suspension and form a sediment bed have been studied very little (Teeter 1986).

14. During depositional formation, depositional flux $C W_s$ must be included in the model dense-suspension height equation:

$$\frac{dH_s}{dt} = \frac{C W_s}{C_{s_i}} - W_{h_i} \quad (D7)$$

where C is the suspension concentration. However, at high deposition rates this equation does not reproduce the observed fluid mud formation very well. Figure D1 shows a plot of the experimentally determined variables which appear in the equation, and shows a disagreement between the observed fluid mud

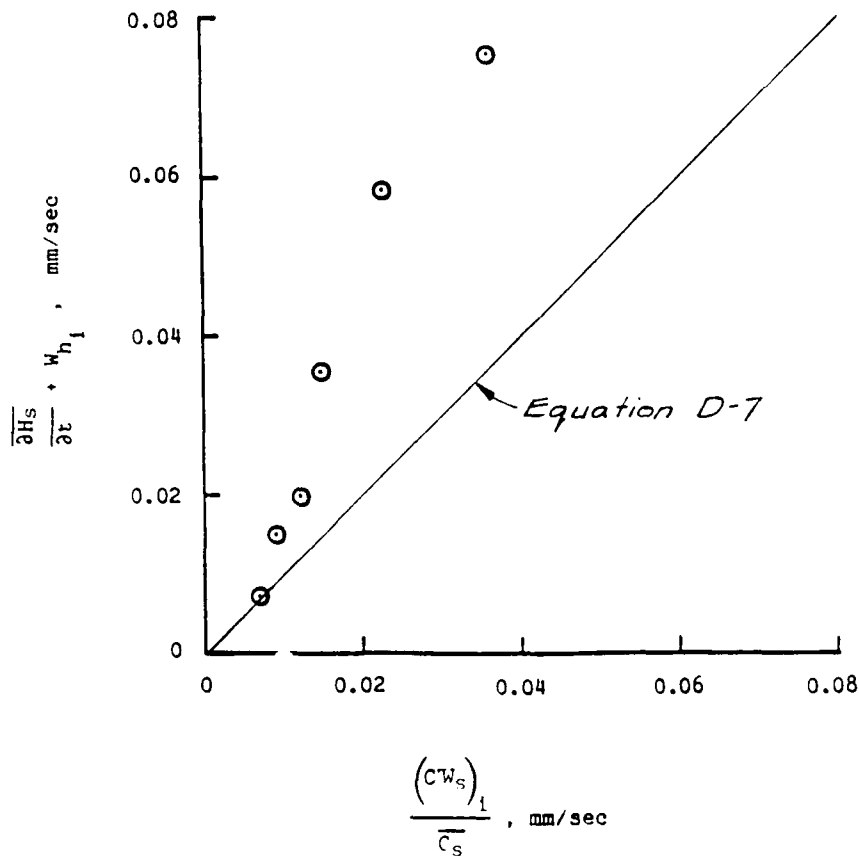


Figure D1. Example experimental data on the terms of Equation D7

characteristics and the equation. Rapid deposition apparently reduces hindered settling in the deposit. At higher concentrations and settling rates the term $C W_s / C_{s_1}$ was closer to $(dH_s/dt) - W_{h_1}$. Therefore, a criterion was used to define the higher depositional range, and that criterion was found to be $dH_s/dt > 2 W_{h_1}$.

15. The upper boundary condition imposed on the transport equation was changed during rapid deposition to

$$C_{s_1} = B3 W_{s_1} \quad (D8)$$

where B3 is an empirical constant. Figure D2 shows a plot of W_s versus initial C_s for tests performed with Corpus Christi sediments.

Verification to laboratory experiments

16. The hindered-settling consolidation model has reproduced observed interface descent for several sediments. Laboratory data from hindered

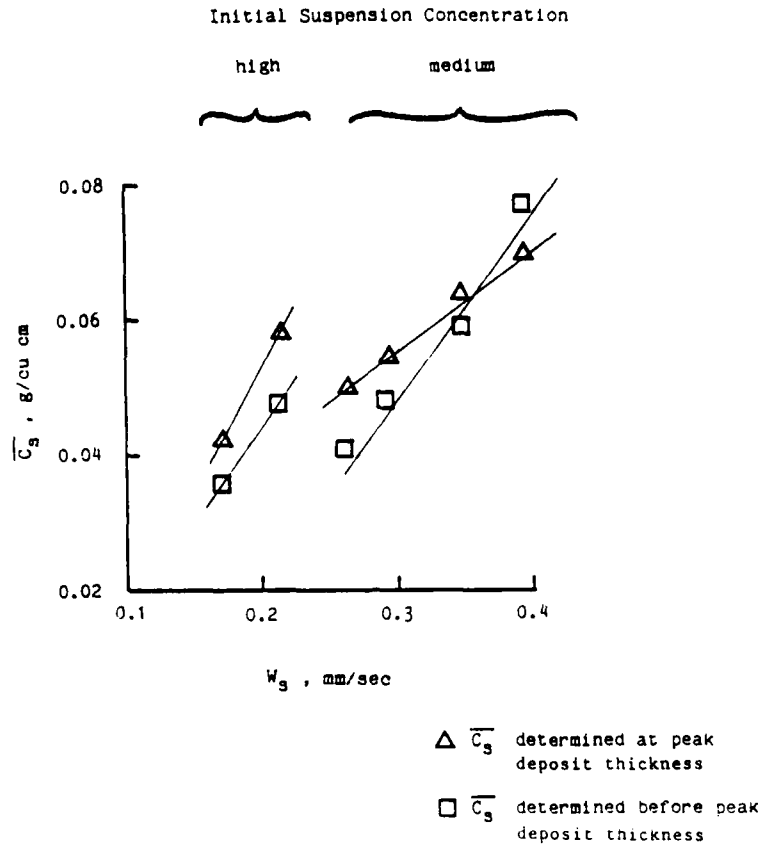


Figure D2. Example experimental data on the relationship between \bar{C}_s at the interface of the dense suspension, and W_s of the overlying suspension

settling consolidation tests were used to fit Equation D1. Figure D3 shows an example comparison between numerical and experimental data for Atchafalaya Bay sediments. The computed vertical concentration profiles were also very similar to those observed during tests. Concentrations increased at the bottom first. The commonly observed inflection in the interface descent occurred in the numerical simulations when the surface concentration first increased. The rate of interface descent was found not to be sensitive to the initial height of the suspension, as reported by several investigators.

17. Results of numerical calculations of fluid mud formation are shown in Figure D4. Both the dense suspension and overlying suspension were modelled using the previously described method for rapid deposition. Note that deposition ceased at about 2.2 hours into the test as the overlying suspension became exhausted of sediment. The dense suspension deposit, which had grown linearly with time, began to consolidate at this point.

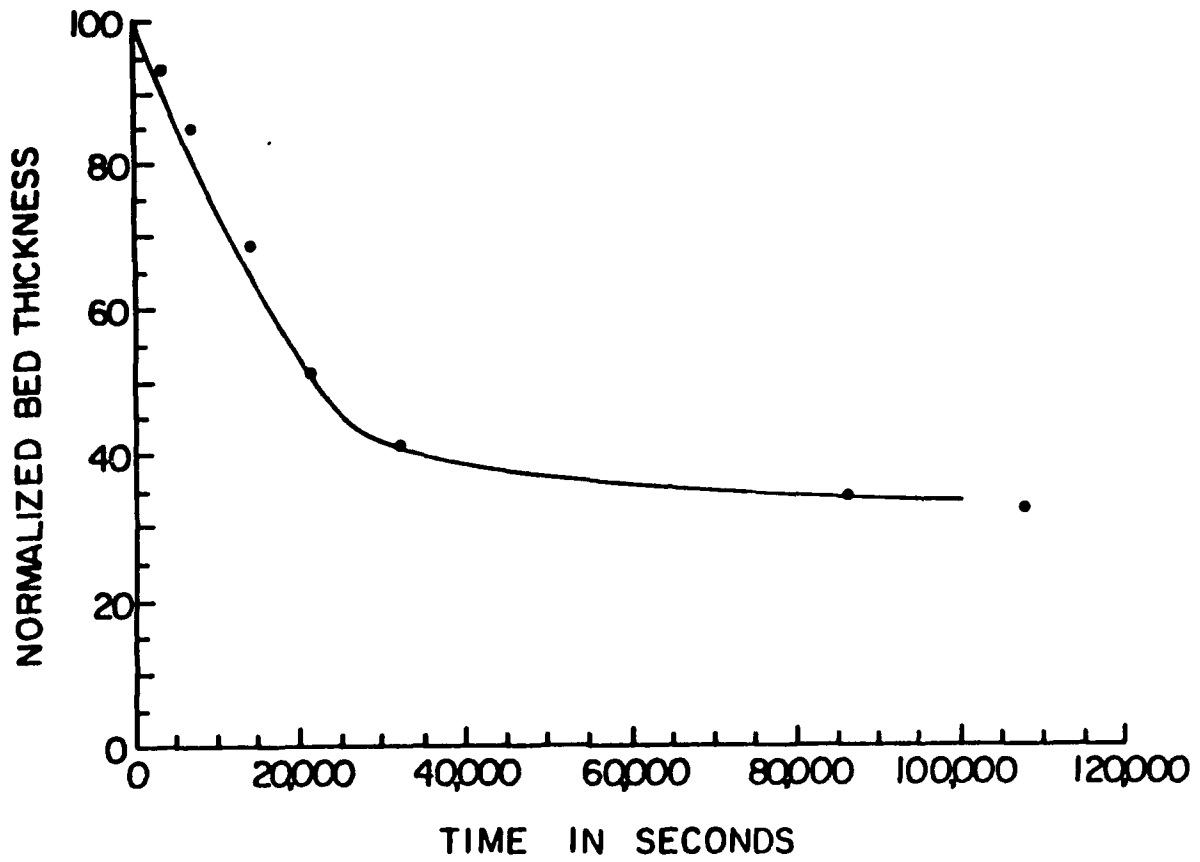


Figure D3. Example comparison between experimental data (·) and model results for the interface height of a hindered-settling consolidation test

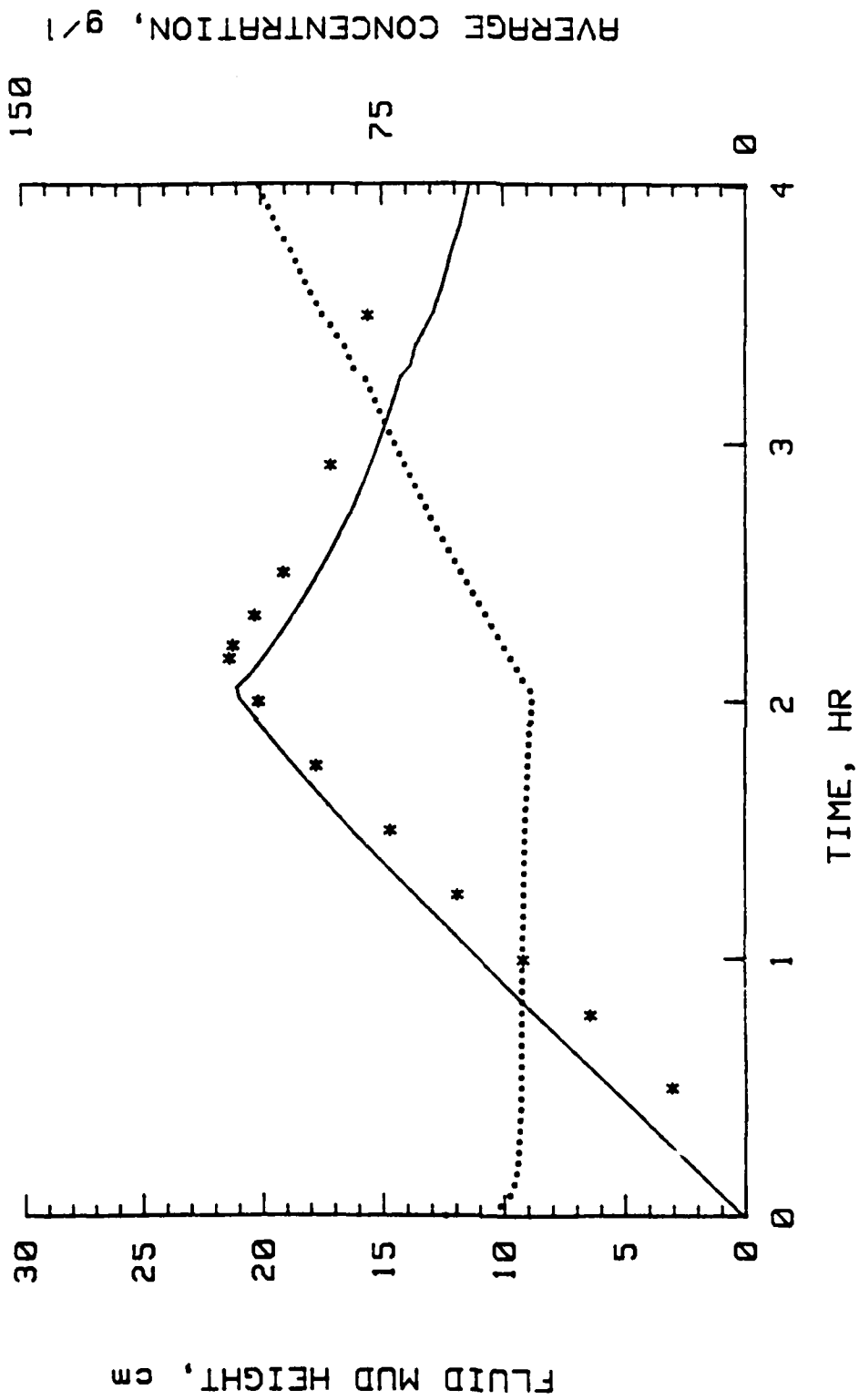


Figure D4. Example comparison between experimental data and model results for the interface height of a deposition and dense suspension formation test

APPENDIX E: DEFINITIONS OF TERMS

Bed	The lower level of the flow field, i.e., the level of no flow
Deposition	Removal to the bed of sediment from suspension by settling.
Flux	The transport of salt or suspended sediment through a certain area. Calculated as the product of velocities, salinities, or suspended sediment concentrations, and cross-sectional or unit areas, and usually summed over a tidal cycle.
Flux components	Statistical correlations calculated by a sequence of time and depth averaging for the purpose of resolving instantaneous and depth deviations in fluxes at a sampling station.
Resuspension	Erosion. The removal of sediment from the bed by the forces of the flow.
Salinity	Concentration by weight (expressed as parts per thousand or ppt) of inorganic matter (mainly chloride, bromide, sodium, potassium, magnesium, and calcium) in seawater or brackish water (dilute seawater).
Settling	The balance between gravitational and viscous forces on suspended particles.
Stokes velocity	A residual flow generated by tide or other long-wave propagation. The difference between Eulerian and Lagrangian tidal-averaged velocities.
Stratification	Vertical salinity and density distributions that stabilize estuarine flows by buoyancy effects, and that inhibit vertical turbulent transport of salinity, suspended matter, and momentum.
Tidal average	The average of a quantity or function over a tidal cycle. In the case of flows or fluxes, the residual of tidal motion.
Tidal hydraulics	Instantaneous flows and water-surface elevations associated with earth/astronomical gravitational effects.
Vertical circulation	Tidal residual flow in the vertical plan characterized in estuaries by upstream flow at the bottom and seaward flow near the surface.

Vertical mixing

The vertical turbulent exchange of salinity and suspended material that is generated by an estuarine flow.

APPENDIX F: NOTATION

Subscripts and indices:

b	Bottom; bed
f	Fresh water
i	Quantities at the suspension/bed interface
j	Sediment fraction index
ℓ	Lateral inflow quantities such as salinity S_{ℓ}
o	Indicates a depth average or vertically homogeneous
t	Time
v	Vertical deviation
x	Horizontal coordinate
z	Depth or vertical coordinate

Parameters:

B	Breadth (width)
B_o	Breadth (width) at water surface
C	Concentration of suspended sediment
Cd	Quadratic friction coefficient
C_s	Concentration of bed sediments
Cw	Shallow-water wave speed
D	Deposition
D_x	One-dimensional unadjusted diffusion coefficient
E	Erosion
H	Instantaneous water depth
H_s	Thickness of a fluid mud or dense suspension
$K_{x,z}$	Horizontal and vertical eddy diffusivity for mass coefficients
M	Erosion rate constant for particle erosion

M_h	Erosion rate constant for significant erosion
$N_{x,z}$	Horizontal and vertical eddy diffusivity for momentum coefficients
P	Probability of erosion
P_k	Production of turbulent kinetic energy
R	Water depth to mean tide level
Ri	Richardson number
S	Salinity
S_l	Salinity of lateral inflow or inflowing from a branch
U	Horizontal (laterally averaged) velocity
W	Vertical (laterally averaged) velocity
W_h	Hindered settling velocity
W_s	Settling velocity
g	Acceleration due to gravity
h	Deviation of the water surface from the mean tide level
k	An index, such as the number of sediment fractions
n	Manning's friction coefficient
q	Lateral inflow rate
x	Nondimensional horizontal coordinate for X
z	Nondimensional vertical coordinate for Z
κ	Turbulent kinetic energy
ρ	Density
ρ_0	Reference density (freshwater)
Δ_e	Element length
τ	Shear stress
ϵ	Dissipation of turbulent kinetic energy